Morphology and dynamics of inflated subaqueous basaltic lava flows

Anne Deschamps, Cécile Grigné, Morgane Le Saout, Samuel Adam Soule, Pascal Allemand, Brigitte van Vliet-Lanoë, France Floc'H

Morphology and dynamics of inflated subaqueous basaltic lava flows

Anne Deschamps[1], Cécile Grigné[1], Morgane Le Saout[1], Samuel Adam Soule[2], Pascal Allemand[3], Brigitte Van Vliet Lanoe[1], and France Floc'h[1]

[1]Université de Brest, UMR CNRS-6538 Domaines Océaniques, Institut Universitaire Européen de la Mer, Plouzané, France, [2]Department of Geology and Geophysics, Woods Hole Oceanographic Institution, Woods Hole, Massachusetts, USA, [3]Laboratoire de Géologie de Lyon-OSU de Lyon, Université Lyon 1 et ENS-Lyon, 2 rue Raphaël Dubois, Villeurbanne, France

Abstract During eruptions onto low slopes, basaltic Pahoehoe lava can form thin lobes that progressively coalesce and inflate to many times their original thickness, due to a steady injection of magma beneath brittle and viscoelastic layers of cooled lava that develop sufficient strength to retain the flow. Inflated lava flows forming tumuli and pressure ridges have been reported in different kinds of environments, such as at contemporary subaerial Hawaiian-type volcanoes in Hawaii, La Réunion and Iceland, in continental environments (states of Oregon, Idaho, Washington), and in the deep sea at Juan de Fuca Ridge, the Galapagos spreading center, and at the East Pacific Rise (this study). These lava have all undergone inflation processes, yet they display highly contrasting morphologies that correlate with their depositional environment, the most striking difference being the presence of water. Lava that have inflated in subaerial environments display inflation structures with morphologies that significantly differ from subaqueous lava emplaced in the deep sea, lakes, and rivers. Their height is 2–3 times smaller and their length being 10–15 times shorter. Based on heat diffusion equation, we demonstrate that more efficient cooling of a lava flow in water leads to the rapid development of thicker (by 25%) cooled layer at the flow surface, which has greater yield strength to counteract its internal hydrostatic pressure than in subaerial environments, thus limiting lava breakouts to form new lobes, hence promoting inflation. Buoyancy also increases the ability of a lava to inflate by 60%. Together, these differences can account for the observed variations in the thickness and extent of subaerial and subaqueous inflated lava flows.

1. Introduction

Basaltic flows spreading through tube-fed systems form lobes that can progressively coalesce and inflate to many times their original thickness over periods of weeks or months due to the steady injection of magma beneath a cooled upper crust. Inflated basaltic lava flows forming remarkably smooth and horizontal features such as tumuli and pressure ridges have been reported in different environments, such as subaerial shield volcanoes in Hawaii, La Réunion and Iceland [e.g., *Walker*, 1991; *Hon et al.*, 1994; *Self et al.*, 1996, 1997], in continental environments such as the US states of Oregon, Idaho, and Washington [e.g., *Hon and Kauahikaua*, 1991; *Chitwood*, 1994; *Thordarson and Self*, 1998], and in the deep sea at the Axial Volcano on the Juan de Fuca Ridge [*Appelgate and Embley*, 1992; *Chadwick et al.*, 2013], on the flat seafloor at the summit of the Galapagos spreading center, 92–95°W [*McClinton et al.*, 2013], and at the summit of the East Pacific Rise at ∼16°N (this study). These lava flows have all undergone inflation processes, yet they display contrasting morphologies that seem to correlate with their depositional environment, the most striking difference being the presence of water.

At the summit of the East Pacific Rise at ∼16°N, inflated lava form tumuli, pressure ridges and large pressure plateaus. Our morphological analysis of these lava flows is based on high-resolution bathymetric data (1 m × 1 m gridded data) acquired using an Autonomous Underwater Vehicle (AUV) and complemented with in situ observations by submersible. Their morphology is similar to inflated lava flows emplaced in terrestrial, subaqueous settings such as lakes and rivers of the western US, or in Icelandic lakes. Their emplacement dynamics (e.g., eruption rate) is assumed to be similar to subaerial Pahoehoe flows in which inflation processes have been well documented [e.g., *Walker*, 1991; *Hon et al.*, 1994; *Self et al.*, 1996, 1997]. However,

basaltic Pahoehoe lava flows that have inflated in subaerial environments such as Hawaii and La Réunion Island, display inflation structures with morphologies that significantly differ from subaqueous lava, with smaller inflation heights and larger inflation feature length scales.

This study investigates the morphology of inflated lava emplaced in subaerial and subaqueous environments. In the deep sea, our study is based on high-resolution bathymetry, photos, and videos. In the United States and Iceland, we utilize high-resolution aerial photographs and digital topographic data (e.g., airborne lidar). We also investigate the ambient conditions during their emplacement, i.e., evidence subaqueous eruption. Finally, this study addresses the role of water in lava inflation dynamics, and demonstrates that the presence of water (either in the deep seafloor or a lake or a river) during lava emplacement is a key factor controlling the final size and morphology of inflated flows.

2. Lava Flow Inflation Process

At the onset of subaerial eruptions, basaltic Pahoehoe lava initially form thin (10–20 cm) flows, which form small lobes that progressively coalesce. The single molten unit resulting from this interconnection can swell to many times its original thickness (i.e., several meters) over periods of weeks or months due to the steady injection of magma beneath a solid cooled upper crust. As the lava spreads laterally over subhorizontal ground, the flow advance eventually ceases when its crust develops sufficient "strength" and to counteract the internal hydraulic pressure [e.g., *Macdonald*, 1953; *Walker*, 1991; *Hon et al.*, 1994; *Self et al.*, 1998; *Kauahikaua et al.*, 1998; *Hoblitt et al.*, 2012]. Inflating flows in subaerial environments have been observed to lift heavy objects such as cars [*Hon et al.*, 1994]. When only few lava tubes remain active, they can inflate and eventually form a chain of tumuli and pressure ridges. Sustained injection of magma can increase the hydraulic pressure within the flow front and cause a rupture and new lava breakouts. The surface of inflated flows is typically subhorizontal. Lava flow inflation commonly occurs in areas with very gentle slopes (<2°) [e.g., *Self et al.*, 1996, 1997], and requires long-lasting and moderate effusion rates [e.g., *Hon et al.*, 1994; *Chadwick et al.*, 1999].

Tumuli and pressure ridges a few meters high are diagnostic features of flow inflation [e.g., *Walker*, 1991; *Chitwood*, 1994; *Rossi and Gudmundsson*, 1996; *Duraiswami et al.*, 2001]. A tumulus is a circular to oval mound with tilted sides, and that is cut by axial and radial inflation clefts or fractures, caused by the upward bending of the crust during swelling [*Walker*, 1991]. A tumulus develops over a clogged part of an active lava tube with enough internal pressure to raise its roof upward. Elongated tumuli may grade into pressure ridges elongated in the direction of the feeding lava tube [*Walker*, 1991]. One or several inflation clefts often develop along their crests.

Flow inflation can also result in a pressure plateau that displays subhorizontal surface and sides composed of outward-tilted slabs of crust. Inflation clefts usually develop around its perimeter. A pressure plateau can reach 1.5 km in length, with a thickness ranging 1 m–21 m [*Chitwood*, 1994]. Circular or irregularly shaped depressions bounded by steep sides are often observed within pressure plateaus. These "plateau pits" (or "lava-rise pits") correspond to regions that did not inflate due to preexisting topographic highs or obstacles that were not covered by the initial, thin lava flow or not sufficiently covered to inflate with the rest of the lava forming the plateau [*Chitwood*, 1994].

Although inflated flows often solidify without significant lava drainage [*Chitwood*, 1994], they can sometimes deflate dramatically due to a breakout that drains the flow before it solidifies. Deflation occurs when the hydraulic pressure exceeds the strength of the confining crust, typically at the base of the flow. Deflation can also occur when the molten lava drains back into the source vent, the solid crust remaining intact.

Pahoehoe lava is able to inflate due to the development of a viscoelastic layer covered by a brittle crust of cooled lava [e.g., *Hon et al.*, 1994] that is able to constrain the flow advance while permitting stretching and local inflation of lava lobes. Eruption temperature of tholeiitic basalts ranges 1140–1200°C [e.g., *Sakimoto and Zuber*, 1998; *Cashman et al.*, 1999; *Soule et al.*, 2004; *Helo et al.*, 2013; *Garel et al.*, 2012] and solidus temperature ranges 990–1100°C [e.g., *Turcotte and Schubert*, 1982; *Griffiths and Fink*, 1992b; *Hon et al.*, 1994; *Rowland et al.*, 2003; *Wantim et al.*, 2013]. Radiative cooling leads to the formation of a thin glassy rind at the flow surface, with the glass transition being estimated at ∼730°C for basalts [e.g., *Ryan and Sammis*, 1981; *Griffiths and Fink*, 1992a]. At the onset of an eruption, the magma behaves essentially as a Newtonian
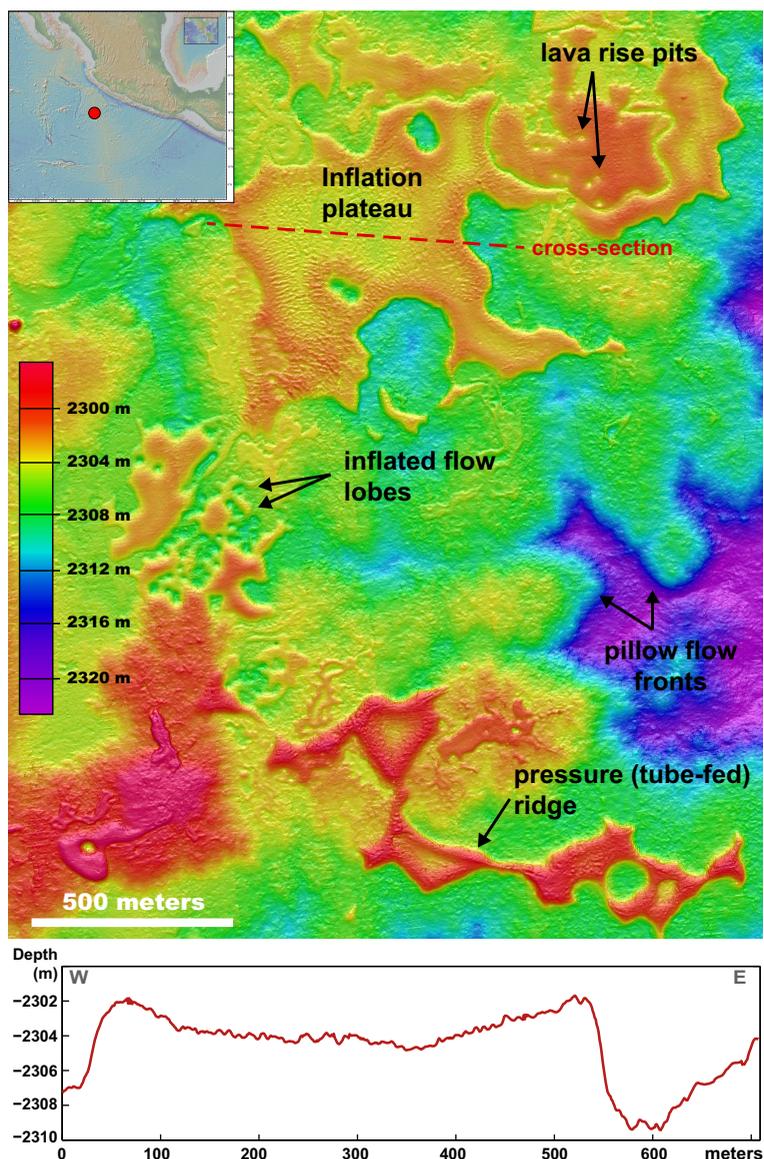
Figure 1. High-resolution bathymetry acquired by the Autonomous Underwater Vehicle Aster-X (Ifremer) of the summit of the East Pacific Rise at 16°N, showing inflated lava lobes, inflation plateaus, and pressure ridges. A bathymetric profile across an inflation plateau, ∼550 m in diameter and ∼8 m in height, is shown. It basin-sag surface shape likely reflects flow deflation.

fluid [e.g., *James et al.*, 2004]. Cooling of the flow unit forms a brittle crust at the surface when the temperature drops below 800–900°C [e.g., *Ryan and Sammis*, 1981; *Wright and Okamura*, 1977; *Hoblitt et al.*, 2012]. As the cooling front progresses inward, the zone of crystallization thickens, forming a viscoelastic skin whose yield strength is able to retain the incoming lava. The thickness of the skin depends on the depth of the ∼1070°C isotherm [e.g., *Hon et al.*, 1994; *James et al.*, 2004]. The positive correlation between the thickness of this crust and the square root of time during which inflation occurs is described by *Hon et al.* [1994], based on direct measurements from the Kupaianaha basaltic lava field, Hawaii.

3. Inflated Flows at the East Pacific Rise

Lava flows at the summit of the East Pacific Rise (EPR) between 15°22′N and 16°15′N have been mapped during the 2010 PARISUB cruise using the R/V L'Atalante, the Autonomous Underwater Vehicle (AUV) AsterX, and the manned submersible Nautile (Ifremer; Figure 1). Near-bottom, high-resolution (1 m × 1 m
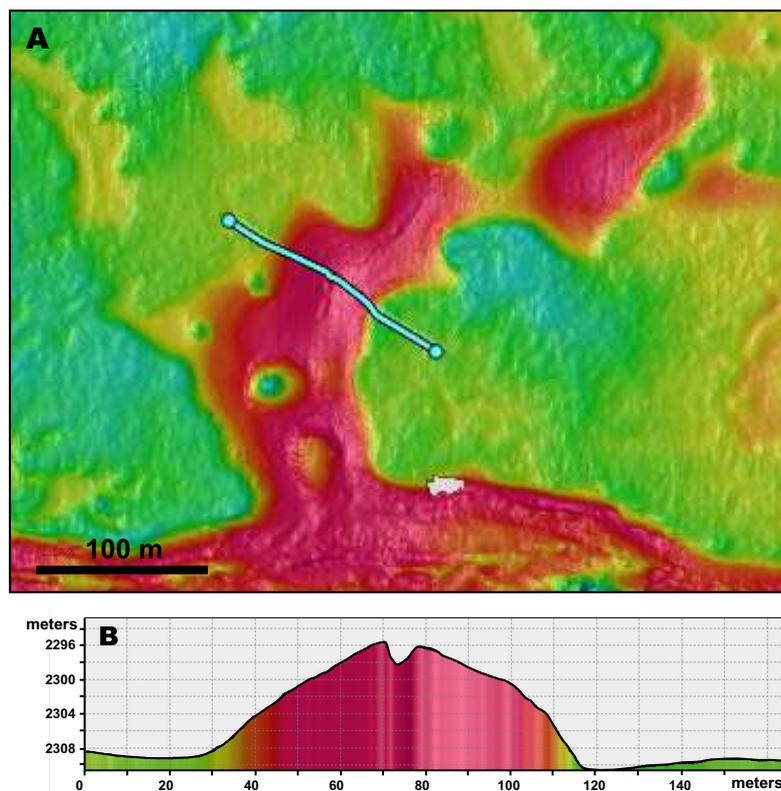
Figure 2. A 2-D view and cross section of a pressure ridge and inflated lava flow lobes at the summit of the East Pacific Rise (16°N), showing the several meters—wide and deep axial crack (or inflation cleft).

gridded) bathymetry acquired by the AUV at 2400 m depth is used to map lava flow boundaries and to quantify their morphological characteristics. Photos and videos acquired during submersible dives are used to investigate the surface texture of the flows. The 16°N segment, spreading at a rate of 87 mm/yr, is the shallowest and the widest of the EPR due to enhanced volcanism as result of its interaction with the Mathematician hotspot [e.g., *Scheirer and Macdonald*, 1993; *Cormier et al.*, 1995; *Wang et al.*, 1996; *Carbotte et al.*, 2000]. It is characterized by a wide axial plateau, the low slopes of which constitute an ideal place for flow inflation.

At the summit of the EPR, lava tumuli, inflated plateaus, and tube-fed pressure ridges are present on the 6–10 km wide flat surface of the axial plateau that surrounds the axial volcanic ridge (Figures 1 and 2). Inflation plateaus display lobate edges, and photos and videos indicate a smooth surface texture (Figure 3). They are primarily composed of jumbled and lineated sheet flows with occurrences of pillow flows at their margin and at their base. Inflation plateaus are 5–15 m high, and their surface areas 0.2–1.5 km^2. Their surface is either planar or depressed (Figure 1). Depressions likely reflect a decrease in hydrostatic pressure within the lava core lava during eruption due to lava draining into the eruptive fissure or due to a breakout at the flow margin to emplace a further lobe. A series of clefts, up to several meters in depth (Figures 2 and 3), parallel the sinuous edges of the plateaus and separate their horizontal surface from their inclined flanks (15–45°) that are composed of strongly outward-tilted planar slabs of lava (Figure 3). The depth of the inflation cleft is likely underestimated due to the insufficient resolution of bathymetry data. Lava-rise pits, up to 70 m in diameter, and 8 m deep, are observed within inflation plateaus. Tumuli reach 8 m in height. They are characterized by steep flanks (up to 65°) and an exceptionally smooth surface texture (Figure 3). Sinuous pressure ridges, 30–120 m wide, up to 1 km long and to 15 m high, some of which display longitudinal medial inflation clefts, reflect the existence of lava tubes [e.g., *Fornari*, 1986; *Appelgate and Embley*, 1992].

The shape of inflated structures, their surface texture and the fact that they overlie a subhorizontal floor (always <2°), suggest that they were emplaced as subhorizontal sheets of lava that swelled due to a sustained magma injection beneath cooled crust formed at the surface of the flow. The basin-sag shape of
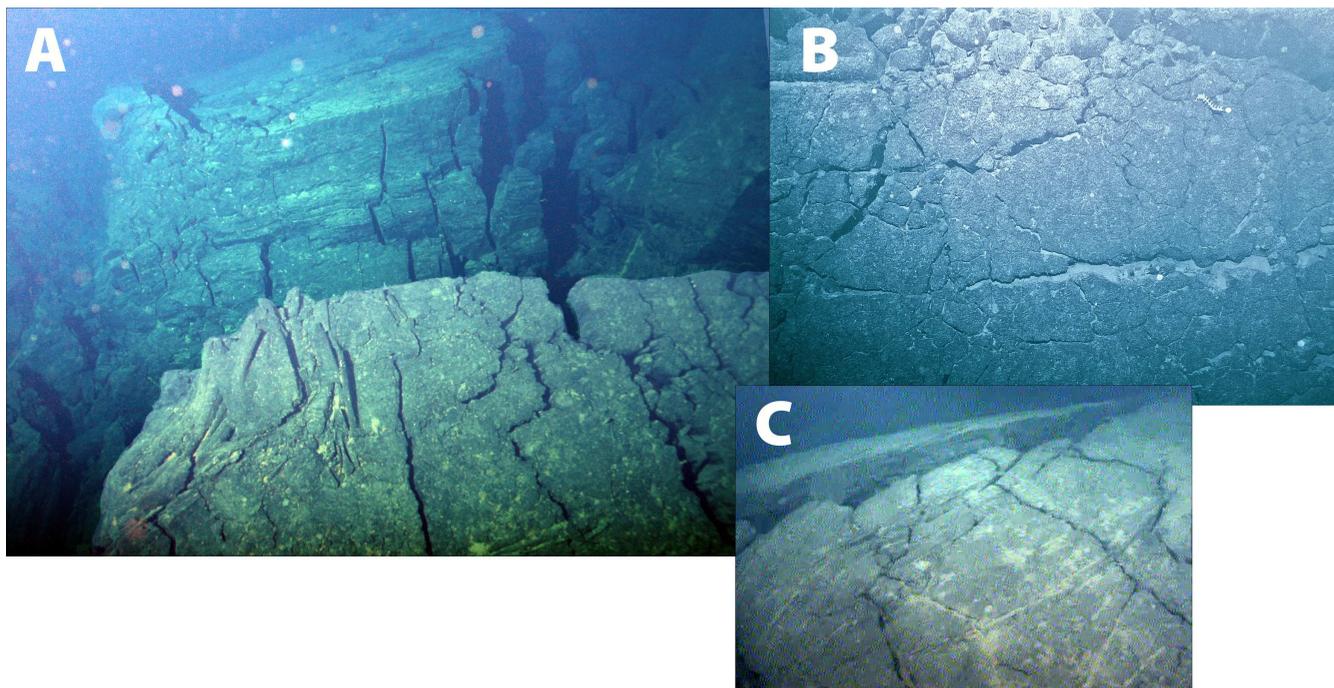
Figure 3. Photo of inflated features at the summit of the East Pacific Rise, 16°N, taken by the manned submersible Nautile (Ifremer) during the Parisub cruise onboard the R/V L'Atalante in 2010. (a) Inflation clefts at the summit of a tumulus (15°42′23″N/105°25′59″W); (b) steep (slope > 60°) smooth flank of a tumulus (15°43′43″N/105°26′17″N); and (c) surface of an inflated lobe (15°42′07″N/105°25′54″N).

plateaus is likely due to episodes of deflation related to the extrusion of new lobes at margin breakouts. Such lobes display pillow lava at their margins. Some tumuli and inflated lobes remain isolated, not apparently connected with any other inflated flow lobes (Figure 1), and confirming the existence of a complex tube system within the flow, connected to the eruption source [*Walker*, 1991].

Similar submarine inflated lava have been observed based on side-scan sonar at Axial Volcano on the Juan de Fuca Ridge [*Appelgate and Embley*, 1992; *Chadwick et al.*, 2013]. Authors observe inflated lobes of several hundred meters in diameter, and 75–100 m wide and 650 m long pressure ridges. They also observe 3–7 m wide planar slabs of lava at the flow margins, sloping down from the top of the flow at angles ranging 45–90°. When observed, inflation clefts 0.5–1 m deep separate the upper surface of the flow from their tilted flanks. Inflated flows with morphological characteristics that seem to be similar to that of the East Pacific Rise and Juan de Fuca Ridge are also observed on a flat seafloor at the summit of the Galapagos spreading center, 92–95°W [*McClinton et al.*, 2013].

4. Subaerial Inflated Pahoehoe Flows (Hawaii and La Réunion Islands)

On Hawaii's Kilauea volcano, inflated Pahoehoe flows emplaced on subhorizontal surfaces have been well documented [e.g., *Hon et al.*, 1994]. They form smooth flat-topped flows with margins displaying tilted outward-dipping lava slabs and vertical fissures. During the eruption of Mauna Ulu on Hawaii (1969–1974), a Pahoehoe flow swelling to about 4 m was observed [*Holcomb*, 1981]. *Hon et al.* [1994] monitored flow inflation during several eruptions at Kilauea. They observed the coalescence and inflation of originally 10–50 cm thick Pahoehoe lobes to 1.5 m (for the flow emplaced in January 1988) and 4 m (for the April 1990 flow) over periods of 50–120 h, respectively. The April 1990 flow reached 65% of its maximum thickness during an initial 10 h period. Although most of the inflation occurs during the first hours of eruption, flows can continue to inflate at a much slower rate over several years, until it eventually freezes [*Hon et al.*, 1994].

Inflated lava flow features are also observed on La Réunion Island, France. A large (11 km^2) transitional olivine basalt Pahoehoe flow field emplaced between the 1750s and the 1790s, on a relatively flat area on the northwestern part of the cone of Piton de la Fournaise, in "L'enclos Fouqué" [*Lénat et al.*, 2001] (Figure 4). Pahoehoe lava texture is generally smooth to ropy. Tumuli up to few meters high and up to ~20 m in

Figure 4. Inflated Pahoehoe lava in the "Enclos Fouqué," Piton de la Fournaise, La Réunion Island (France) (2011). Author: A. Deschamps.

length are observed. The largest pressure ridges reach ∼150 m in length and 30 m in width. Field observations reveal that these tumuli and pressure ridges are a few meters high (but often less than 4 m) and generally less than 15 m in length (Figure 4). No inflation plateaus are observed.

5. Inflated Flows Emplaced in Subaqueous Environments

Flows emplaced subaqueously (e.g., in rivers and lakes) but now emerged, display inflation structures such as tumuli, inflation plateaus and pressure ridges and are exposed in many places around the world, e.g., Washington (ex. Columbia River Basalts), Idaho (ex. Hells Half Acres, Cerro Grande, Craters of the Moon, Wapi flows), Oregon (ex. Badlands, Potholes, Devils Garden, Diamond Craters, Deschute River, Owyhee River, Jordan Crater flows), New Mexico (ex. Cibola, Zuni-Bandera flows), and also in Scotland (ex. Port Haunn, northwest Mull) and Iceland (ex. Lake Mytvan, Budahraun flows in Snaefellness). For example, an Early Tertiary (62–58 Ma) [*Pearson et al.*, 1996], 16–30 m thick inflated lava flow at Port Haunn (northwest Mull, Scotland), was emplaced in a gentle topographic depression, the base of the flow is presently still below the sea level in some places [*Kent et al.*, 1998]. Field studies find evidence for lava tubes, lobes, and vesicle distributions characteristic of inflated flows. Hyaloclastiste at the base of the flow indicates that the flow was emplaced under water [*Lyle*, 2000]. This flow unit far exceeds the thickness of subaerial inflated Pahoehoe flows, a trait common to subaqueous and submarine inflated flows.

We investigate the morphology of several of these presently emerged inflated flows originally emplaced underwater, looking specifically at their morphology and depositional environment. Based on high-resolution aerial photographs and Lidar (Light Detection and Ranging) topographic data, the morphology of these flows is much more similar to lava flows emplaced at the East Pacific Rise than with subaerial inflated Pahoehoe flows observed in Hawaii and La Réunion Island. Based of previous studies, there is abundant evidence for lava-water interaction during flow emplacement such as coeval phreatomagmatic eruptions, or fluvial and lacustrine deposits interbedded with basalt flows, for example.

In order to analyze the morphology of the lava flows that are located in United States, we used the Digital Elevation Model (DEM) based on Lidar data from the National Elevation Dataset (NED) of USGS (United States Geological Survey), with a resolution of 1/9 arc-second (about 3 m) (http://lidar.cr.usgs.gov/). In addition, we use high-resolution orthorectified images that combine the image characteristics of an aerial photograph with the geometric qualities of a map (pixel resolution of 1 m or finer). These images are delivered

DESCHAMPS ET AL.　　　　　　2133

Table 1. Main Characteristics of the Basaltic Quaternary Lava Fields of Central and Southeast Oregon, after *Chitwood* [1994][a]

Flow Name	Badlands	Devils Garden	Potholes	Jordan Craters	Diamond Craters
Emplacement slope (°)	0.8	0.6	0.5	**0.9**	**0.5**
Flow extent (km^2)	75	86	65	**65**	**67**
Volume (km^3)	1.4	1.2	0.96	**1.0**	**1.0**
Thickness (m)	19	15	15	**15**	**15**
Age (years)	300,000	20,000	50,000	**3200**	**17,000**

[a]Lava flows discussed in the text are indicated in bold.

by USGS (https://lta.cr.usgs.gov/). We used the Fledermaus software package to drape the ortho-images on DEMs and to explore the geometry of inflated structures.

5.1. Miocene Inflated Lava of the Columbia River Igneous Province, United States

The 16.5–6 Ma Columbia River Basalts (CRB) cover an area of 200,000 km^2 in Washington, Oregon, and Idaho [e.g., *Self et al.*, 1996; *Hooper*, 1982, 2000]. CRB flows are dominantly Pahoehoe-like sheet lava with thicknesses ranging 15–50 m and volumes ranging 100–1000 km^3. They were emplaced on gentle slopes (<0.1%) [e.g., *Swanson et al.*, 1975; *Tolan et al.*, 1989; *Self et al.*, 1996]. Most of the CRB lava underwent inflation by continuous injection of basalt into slowly moving lava lobes [*Self et al.*, 1996, 1997] as shown by the presence of tumuli, inflation clefts, lava-rise pits [e.g., *Hon and Kauahikaua*, 1991; *Self et al.*, 1991, 1996; *Thordarson and Self*, 1996; *Cashman and Kauahikaua*, 1997]. Pillow lava are commonly observed at the base of the flows [e.g., *Schmincke*, 1967; *Walker*, 1992] attesting for their emplacement into water [*Jones*, 1968]. Based on the cooling model of *Hon et al.* [1994] for Hawaiian inflated sheet flows, *Self et al.* [1996] calculated that 2.7 years are required to form the ~12 m thick surface crust in a typical 30 m thick CBR flow.

5.2. Inflated Flows in the Quaternary Lava Fields of Central and Southeast Oregon

Inflated basaltic lava flows are observed in Oregon in the Quaternary lava fields of the badlands [*Bergquist et al.*, 1990], Devils Garden [*Keith et al.*, 1988; *Chitwood*, 1990], Diamond Craters [*Peterson and Groh*, 1964; *Brown*, 1980], Jordan Craters [*Calzia et al.*, 1988], and Potholes [*Jensen*, 2006]. These inflated flows formed when fluid basaltic lava spread out as thin layers (20–30 cm) onto subhorizontal terrain (slope <1°), developing tube-fed systems, and swelling 1.5–19 m (Table 1) [*Chitwood*, 1994]. In this paper, we present the examples of Jordan and Diamond Craters volcanic landforms.

5.2.1. The Jordan Crater Lava Flow near the Cow Lakes, Southeast Oregon

The Jordan Craters lava flow is the youngest of a large Quaternary olivine basalt field in Southeast Oregon. It is located at 43.1°N/117.4°W on the Owyhee-Oregon Plateau, in the vicinity of the Owyhee River. This 75 km^2 (>1.5 km^3) Pahoehoe flow was emplaced ~3200 years ago near Cow lake. It erupted from several source vents, the main vent being the Coffeepot Crater (Figure 5). The flow displays ropey and shelly surfaces, lava tubes, pressure ridges, and lava-rise pits. Pyroclastic activity occurred during lava emplacement as shown by the presence of cinder cones [*Otto and Hutchison*, 1977; *Hart and Mertzman*, 1983].

The lava flowed southeast from the Coffee Pot Crater, creating a natural dam at the origin of two lakes (the Upper and Lower Cow lakes) at the southern end of the lava field. Lava was emplaced in two stages: initial strombolian eruptions produced tephra and spatter cones and was followed by voluminous outflows of lava creating a lava pond, with limited phreatomagmatic activity. These flows show excellent examples of inflated lava structures emplaced in a subaqueous environment.

DEM and orthoimages (Figures 5 and 6) reveal inflation plateaus with diameters of 100–700 m and heights of 2–10 m. Their upper surface is subhorizontal, always sloping less that 0.15°. Sinuous pressure ridges, 30–100 m wide, 1–11 m in height, and up to ~800 m in length are observed.

5.2.2. The Diamond Crater Lava Flow Field, Southeastern Oregon

The Diamond craters volcanic field is located 43.1°N/118.7°W, in Harney County (Southeastern Oregon), on the Oregon Plateau southeast of the Jordan Craters volcanic system, within the Malheur lake drainage basin. Eruptions took place ~7300–7800 years ago, with eruptive activity lasting at least 10–20 years, producing ~1.6 km^3 of lava covering an area of ~70 km^2 [e.g., *Russell and Nicholls*, 1987; *Sherrod et al.*, 2012]. Olivine tholeiite basalts emitted from a fissure system [e.g., *Hart et al.*, 1984] producing Pahoehoe lava flows with
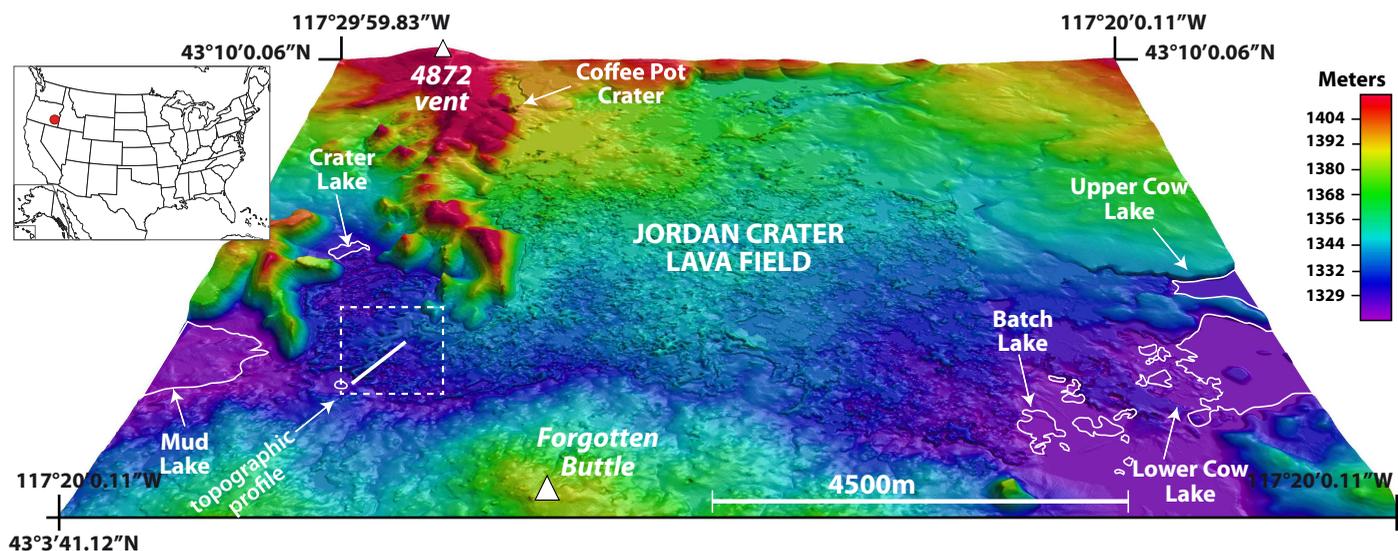
Figure 5. (a) A 3-D view of the topography of the Jordan Crater lava field, southeast Oregon. The map is derived from a 10 m light detection and ranging (LiDAR) digital elevation model. The location of the main source vent, the Coffee Pot Crater is indicated. Lava flowed to the southeast, creating a natural dam in the drainage system, resulting in the formation of the Upper and Lower Cow lakes (positions indicated in white). Data source: National Elevation Dataset of United States Geological Survey. The location of the topographic cross section shown on Figure 6 is indicated in red.

smooth, wrinkled, or ropy surfaces. Numerous tumuli and lava tubes are visible within the lava field. Phreatomagmatic and strombolian activities produced explosion craters, lapilli, scoria cones, and maars (Figure 7) [*Wood and Kienle*, 1992].

The Diamond Crater lava field is underlain by floodplain (alluvial) silts, approximately 7790 years old. In the Pleistocene, the water level in the Malheur Lake was elevated, overtopping the basin's eastern threshold several times and spilling into the Malheur River, a tributary of the Columbia-Snake river system [*Dugas*, 1998]. During eruptions, the lava flows modified the drainage system of rivers [*Sherrod et al.*, 2012].

Within the Pahoehoe lava field, sinuous pressure ridges, 30–140 m wide, and up to 1900 m in length are observed. Inflation plateaus are 150–1200 m in diameter and 2–11 m in height (Figures 7 and 8). Their upper surface is subhorizontal, sloping by less that ∼0.1°.

5.3. Lava Flows of the Owyhee River, Malheur County, Oregon

The Owyhee River is located in Southeast Oregon, draining Nevada, Idaho and the Southeastern Oregon, flowing northward into the Snake River. Over the last 2 million years, the river canyon has been dammed by at least six Pahoehoe lava flows composed of numerous piled up lobes [*Self et al.*, 1998; *Walker*, 1971]. Each flow temporarily blocked the Owyhee River forming lakes before being subsequently incised by the river [e.g., *Orem*, 2010; *Ely et al.*, 2012]. The three best-preserved lava dams and associated lakes are the West Crater (∼70 ka), the Saddle Butte 2 (∼144 ka), and the Bogus Rim lava flows (∼1.9 Ma) [*Bondre*, 2006; *Bondre et al.*, 2004; *Brossy*, 2007; *Orem*, 2010; *Ely et al.*, 2012].

The West Crater lava flow was erupted from the West Crater vent located at 43°N/117°32′W, on the Bogus Bench. The flow followed Bogus Creek to the Owyhee River Canyon, filling the canyon to depths up to 25 m over distances of at least 12 km [*Bondre*, 2006; *Bondre et al.*, 2004; *Brossy*, 2007; *Ely et al.*, 2012]. The dam persisted for at least 25 kyr before incision by the river began. Stratigraphic studies of the lava flow [*Evans*, 1991; *Ely et al.*, 2012] confirm that lava advanced into water, resulting in fluvial and lacustrine sediment sections intercalated with lava lobes, and alternating beds of pillow lava and shattered volcanic glass (hyaloclastite). Within the lava dam, several rising passage zones mark the transition between subaerial and subaqueous portions of the lava flow, and constrain the water surface elevation into which the lava flowed [*Jones and Nelson*, 1970]. These indicate that the water level rose during the formation of the lava dam but did not exceed the lava emplacement rate [*Ely et al.*, 2012].
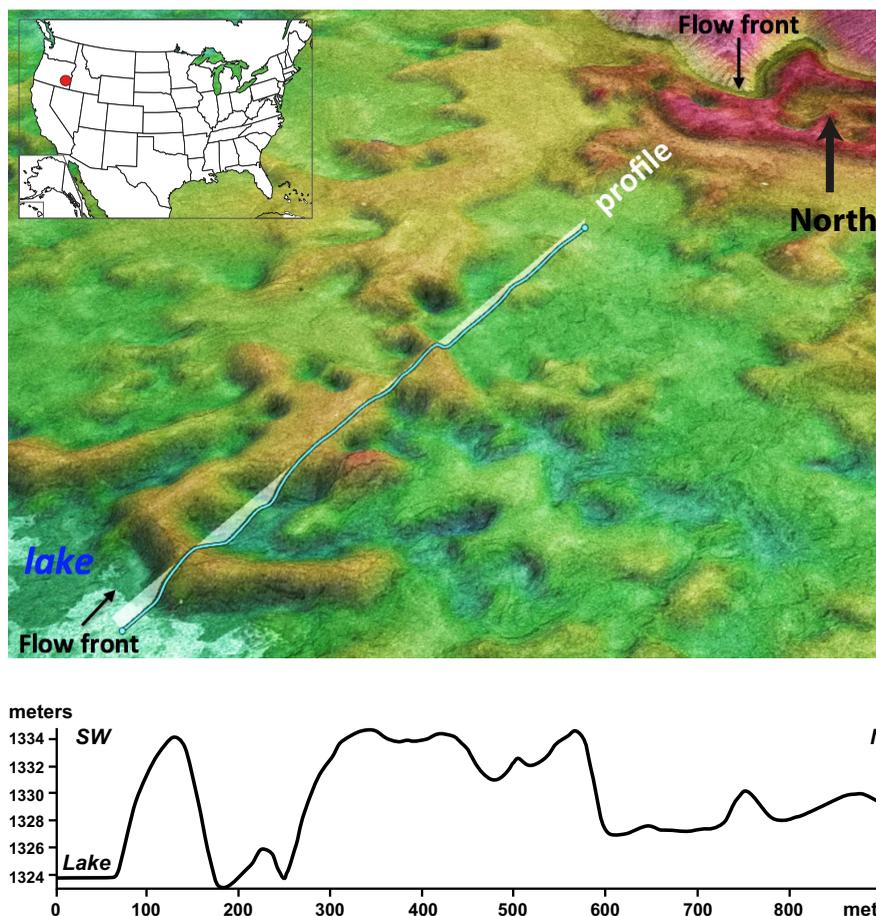
Figure 6. Blowout on the Southwestern flow front of the Jordan Crater inflated lava field, Oregon. (a) A 3-D view of aerial photographs draped on the Digital Elevation Model (DEM) and (b) topographic cross section across a pressure ridge (location is indicated on Figure 4).

The Owyhee River lava field display tumuli and other inflated structures [*Orem*, 2010, 2011] (Figure 9). Inflation plateaus range from 140 to 550 m in diameter, and 2 to 8 m in height, with subhorizontal upper surfaces. Sinuous pressure ridges 30–150 m wide, up to 1100 m long, and 1 and 11 m high meander through the lava field.

5.4. Quaternary Basaltic Magmatism in the Eastern Snake River Plain, Idaho

The Eastern Snake River Plain (ESRP) is a 600 km long and 100 km wide volcanic corridor characterized by basaltic dikes and lava, and phreatomagmatic eruptions related to proximal rivers and lakes. The main Quaternary (Pleistocene to Holocene) basaltic fields are the Hell's Half Acre, Craters of the moon, Wapi, Cerro Grande, and Menan Buttes lava fields [*Hughes et al.*, 1999]. The Snake River was progressively shifted southward by successive ESRP lava flows. Lava fields are composed mainly of olivine tholeiites emplaced as channels or tube-fed Pahoehoe flows, 5–25 m thick [e.g., *Leeman*, 1982; *Greeley*, 1982].

The Hell's Half Acre lava field covers an area of ∼400 km^2 Southwest of Idaho Falls. Pahoehoe flows were emplaced 4100–2000 years ago from a 3 km long, NW-SE trending vent system at the Northwestern part of the field during an eruptive episode lasting a few days to few years [*Kuntz et al.*, 1982, 1992]. Lacustrine, playa, and fluvial sediment lenses and eolian soil blankets are intercalated between the individual flows. The lava field displays channels, tubes, inflated lobes, tumuli, pressure ridges, and lava-rise pits [*Hughes et al.*, 1999]. *Hughes et al.* [1999] note that many lava flow features are similar to inflated sheet flows in Hawaii, having relatively low viscosities and emplaced as coalescing and inflating lobes, but that they experienced inflation at a much larger scale than is typical of Hawaiian Pahoehoe lavas. Flow fronts are several meters thick, and Pahoehoe toes are several tens of meters wide (Figures 10 and 11). Lobes are 5–8 m high,
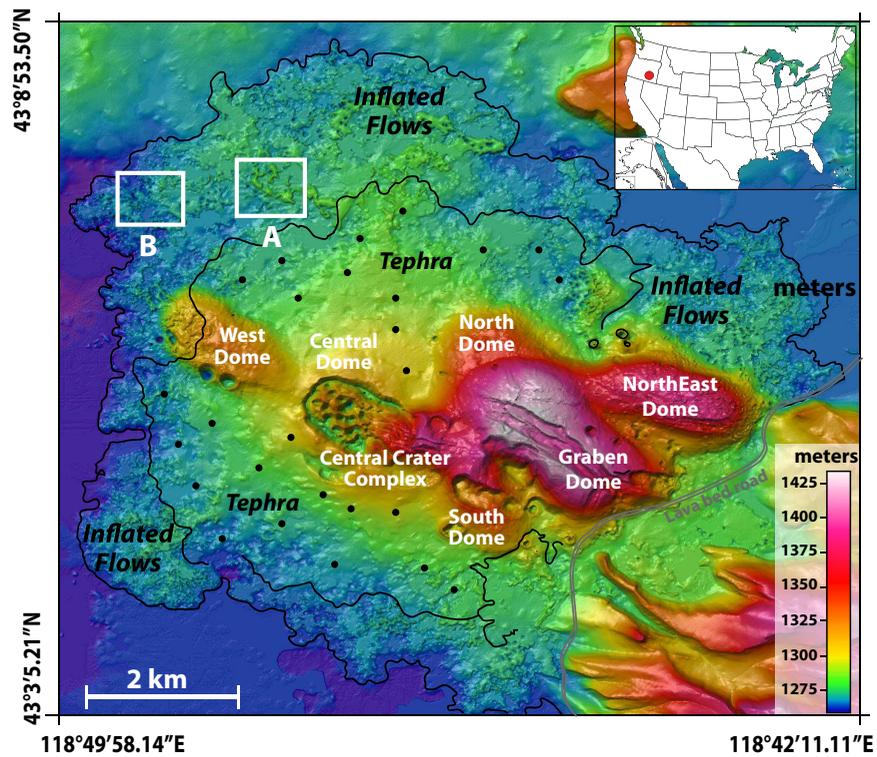
Figure 7. A 2-D view of the topography over the Diamond Crater lava field, southeast Oregon. (a) Map derived from a 10 m light detection and ranging (LiDAR) digital elevation model (DEM). Red rectangles indicate the location of blowouts and cross sections of Figure 8. Data source: National Elevation Dataset (NED) of United States Geological Survey.
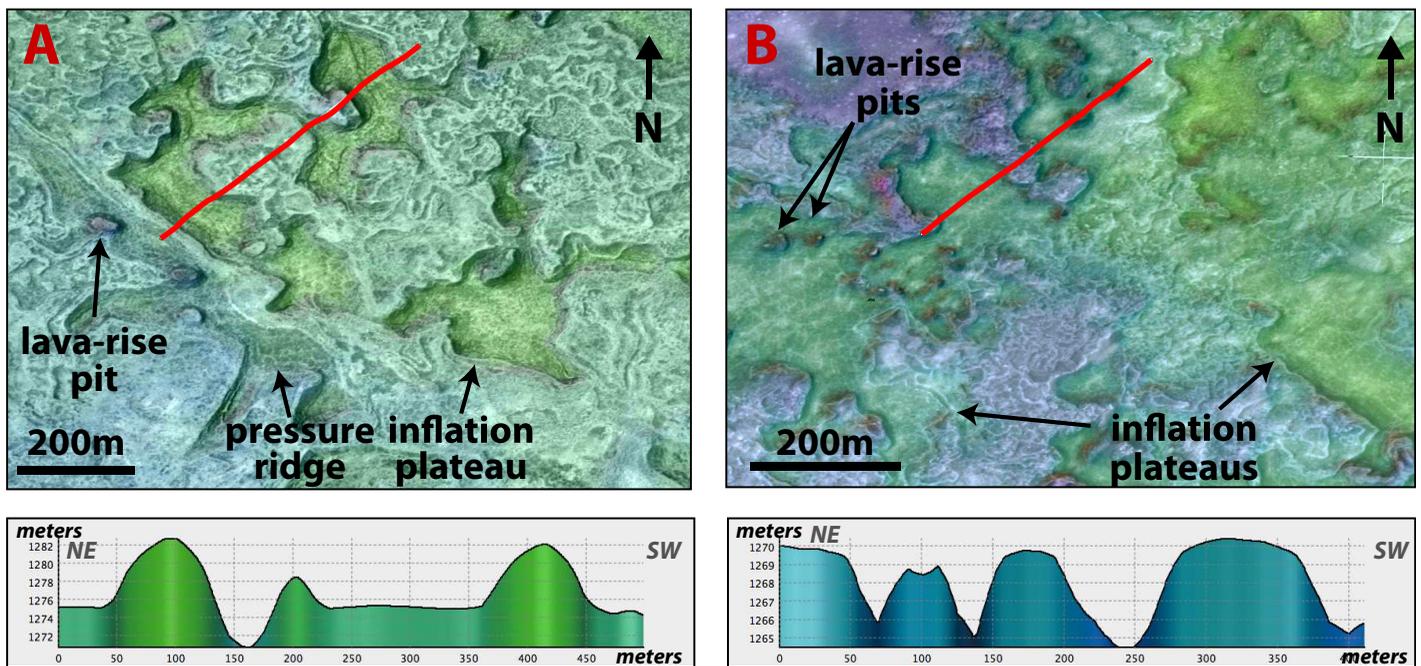
Figure 8. A 3-D views in the northern part of the Diamond crater inflated lava field, Oregon (see location on Figure 7). Semitransparent aerial orthorectified photographs are surimposed on the Digital Elevation Model (DEM). Associated topographic cross sections across inflation plateaus and pressure ridges are shown below. Data source: National Elevation Dataset (NED) of United States Geological Survey.
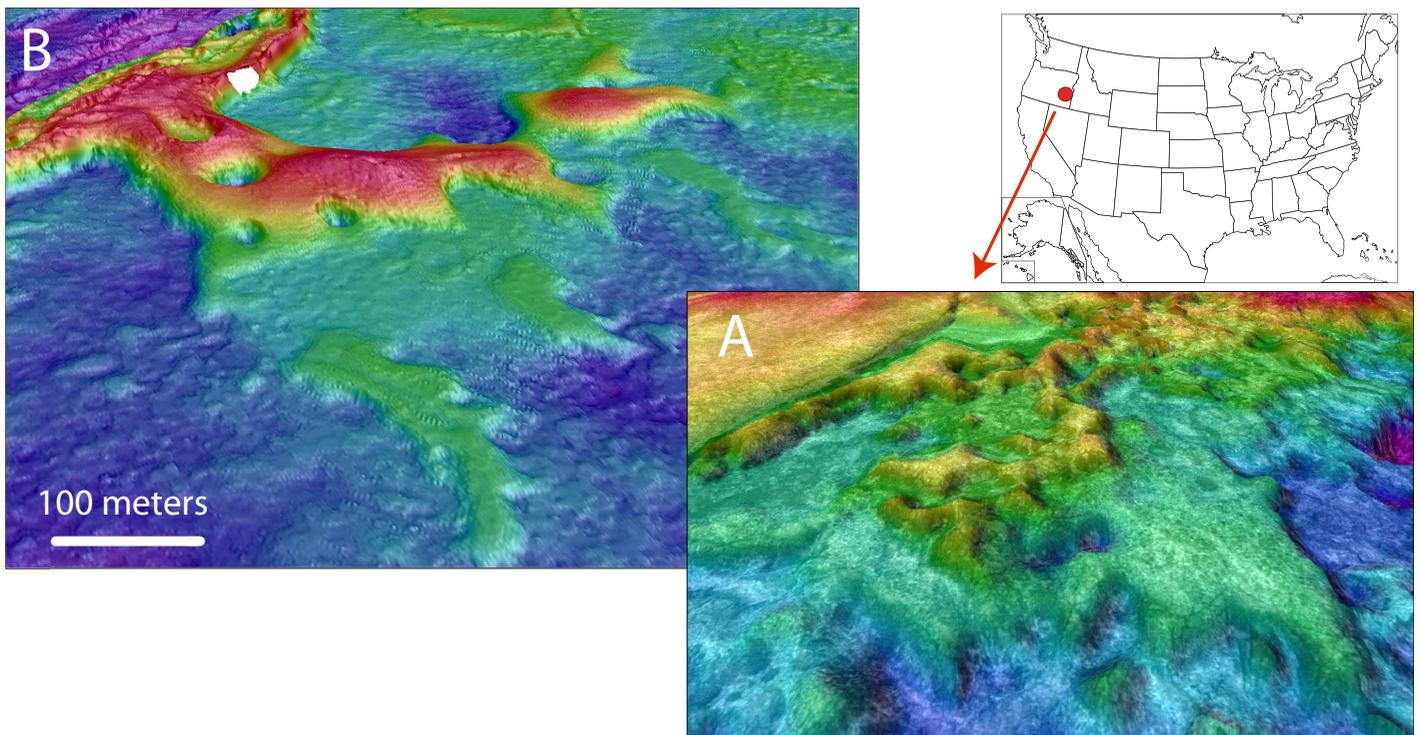
Figure 9. (a) A 3-D view of inflated features of the western part of the Owyhee River lava flow, at the vicinity of the Crater lake, Idaho. The aerial orthorectified photographs are surimposed on the Digital Elevation Model. Data source: National Elevation Dataset (NED) of United States Geological Survey; (b) 3-D view of inflated features at the summit of the East Pacific Rise, 16°N, at the same scale. Data source: high-resolution (1 m cells) bathymetry acquired by the Autonomous Underwater Vehicle Aster-X (Ifremer).
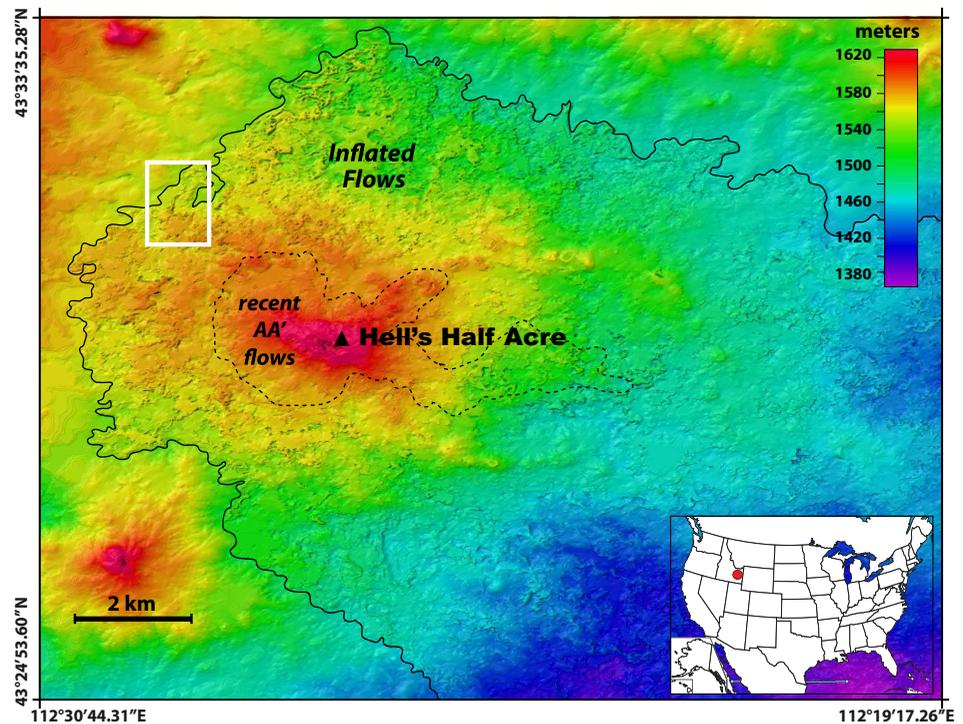
Figure 10. A 2-D view of the topography of the Hell's Half Acre lava field, Idaho, derived from a 10 m light detection and ranging (LiDAR) digital elevation model (DEM). The Pahoehoe lava field is overlain by younger AA lava flows. Location of blowout and topographic cross section on Figure 11 is indicated in white. Data source: National Elevation Dataset (NED) of United States Geological Survey.
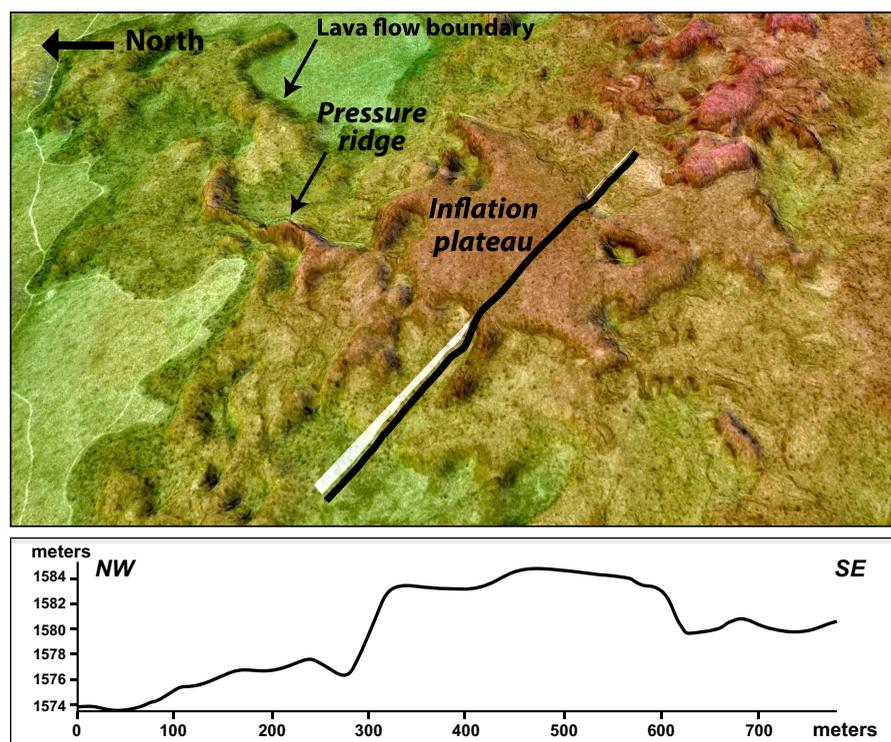
Figure 11. (a) A 3-D view of the topography of the Hell's Half Acre lava field, Idaho, with surimposed semitransparent aerial photographs. The lava field with inflation structures (plateaus, pressure ridges) appears in the darker color. Location on Figure 10; (b) topographic cross section across an inflation plateau. Data source: National Elevation Dataset (NED) of USGS.

and up to 100 m wide. Inflation clefts at the peripheries of the lobes are 3–5 m deep. Some flows display a basin-like sag shape due to deflation as magma broke out from an expanding lobe [*Hughes et al.*, 1999].

5.5. Inflated Subaqueous Basaltic Flows of Iceland

To analyze Icelandic lava flows, this study used photographs from the National Land Survey of Iceland, IS50V database (http://atlas.lmi.is/kortasja/) that gathers GPS road surveying, aerial photographs, and SPOT-5 satellite images, and aerial photographs of Loftmyndir ehf's database (http://www.loftmyndir.is/), which recently unveiled a model of the whole country that is accurate down to the nearest 2 m (resolution up to 1:2000). No DEMs with sufficient resolution are available over the regions of interest so flow unit analysis is based only these images.

Inflated Pahoehoe flows displaying large inflation structures such as plateaus of several hundred meters in diameter are also observed in Iceland. These flows emplaced in subaqueous environments, such as lakes, river beds, or below the sea level but they are presently subaerial. Here we show two examples of such inflated subaqueous flows in Iceland:

5.5.1. Eldá Lava Flow, Northern Shore of the Mytvan Lake

The Myvatn lake, ~4.2 m deep and covering an area of ~37 km², is located in Northeast Iceland, Southwest of Krafla Volcano. The lake has been shaped by the 2500 year old "younger Laxarhraun" lava flow from Mt. Hverfjall. When the lava flowed into lakes and wetlands, steam explosions formed the pseudocraters and rootless cones and the small islands of Myvatn lake, which covered a much larger area than today [*Einarsson*, 1982; *Greeley and Fagents*, 2001; *Mattsson and Höskuldsson*, 2011]. Over the last 250 years, Krafla has been the source of two major volcanotectonic episodes: the 1724–1729 Myvatn Fires and the 1975–1984 Krafla Fires. The Myvatn Fires included a series of four small (<0.2 km³) effusive eruptions [e.g., *Einarsson*, 1991; *Sæmundsson*, 1991] during which rapid water level fluctuations occurred in the Myvatn Lake. The northern part of the lake dried up in 1724 for 9 months, so much so that trout catches dramatically failed [e.g., *Thorarinsson*, 1979; *Olafsson*, 1979; *Einarsson et al.*, 2004]. The younged Myvatn lava (1729) flowed along the Eldá riverbed (herein called the "Eldá lava flow") into the northern part of the lake, now
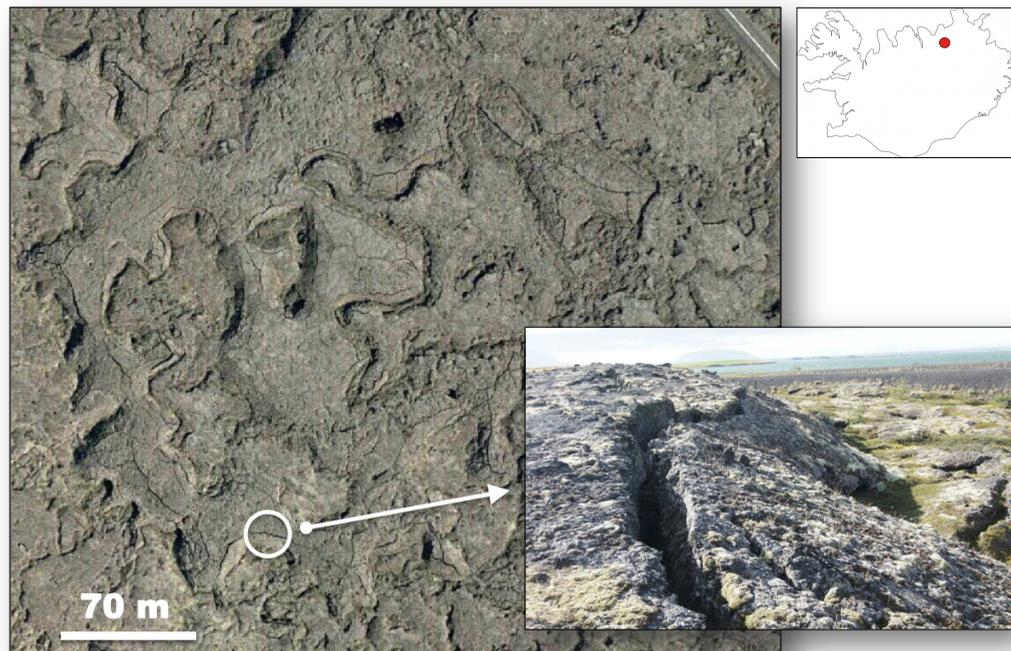
Figure 12. (a) Aerial photograph of the Eldá lava flow emplaced during the Krafla fires in 1724–1729 on the northern shore of the Mytvan Lake, Iceland. Inflation plateaus up to 350 m in diameter, and pressure ridges up to 250 m long are visible. Data source: Loftmyndir ehf's database. (b) Pressure ridge with inflation cleft and tilted flanks. Source: *Deschamps* [2013].

constituting 2.4 km of the shoreline on its Northern border. Historical reports indicate that the lake water reached high temperatures during this eruption, but do not indicate the length of time before the lake returned to normal [*Olafsson*, 1979]. The Eldá lava flow consists of smooth inflated lava. The maximum height for this inflated facies is ∼18 m, which corresponds to lacustrine terraces and the altitude of the lake paleo-outlet on aerial photos. Inflation plateaus are up to 350 m in diameter, and pressure ridge are up to 250 m long (Figure 12).

5.5.2. Brunahraun Lava Flow, Laki Eruptive System

The Laki system, SouthEast Iceland, was active for 8 months in 1783–1784 AD, erupting ∼15 km^3 of tholeiitic basalts from a 27 km long fissure. Lava flowed down the Skaftá and the Hverfisfljót riverbeds, forming a ∼600 km^2 lava field [*Guilbaud et al.*, 2007]. It impeded the drainage from the Vatna ice sheet, inducing temporary lakes within two valleys and local pseudocrater fields (close to Lakigirar and Vatnajökull). It finally spread onto a coastal plain [*Grönvold*, 1984; *Sigmarsson et al.*, 1991; *Thordarson and Self*, 1993; *Thordarson et al.*, 1996; *Thordarson and Hoskuldsson*, 2002]. In June 1783, ∼130 scoria cones related to phreatomagmatic explosions formed due to the groundwater interacting with the rising lava. The lava flow blocked the Skafta River, filling the gorge (up to 100 m deep) [*Steingrímsson*, 1998]. Over a few days the eruptions became less explosive, Strombolian, and later Hawaiian in character. According to *Self et al.* [1998], pulses of inflation and drain out causing new lobes, occurred during at least a few tens of days.

Aerial photographs of inflated Pahoehoe flows in the Hverfisfljót river gorge, ∼300 m to the North-NorthEast the Eyjalon lake (Figures 13 and 14), reveal plateaus several hundred meters in diameter (∼700 m at maximum), with a smooth to platy-ridged upper surface [*Keszthelyi et al.*, 2004]. Lava-rise pits, 3–15 m in diameter, and deep inflation clefts are observed at the surface and at the flow margins. Figures 13 and 14 indicate how the morphology of these flows is similar to the inflated flows in the deep sea, at the summit of the East Pacific Rise.

In conclusion, the morphology of inflation features such as tumuli, pressure ridges, and inflation plateaus of the submarine basaltic lava flows at the East Pacific Rise, and subaqueous lava flows in the Western US and Iceland, indicates that these flows experienced inflationary emplacements at a much larger scale than Pahoehoe flows in subaerial environments such as Hawaii and La Réunion Island. The geometry and size of
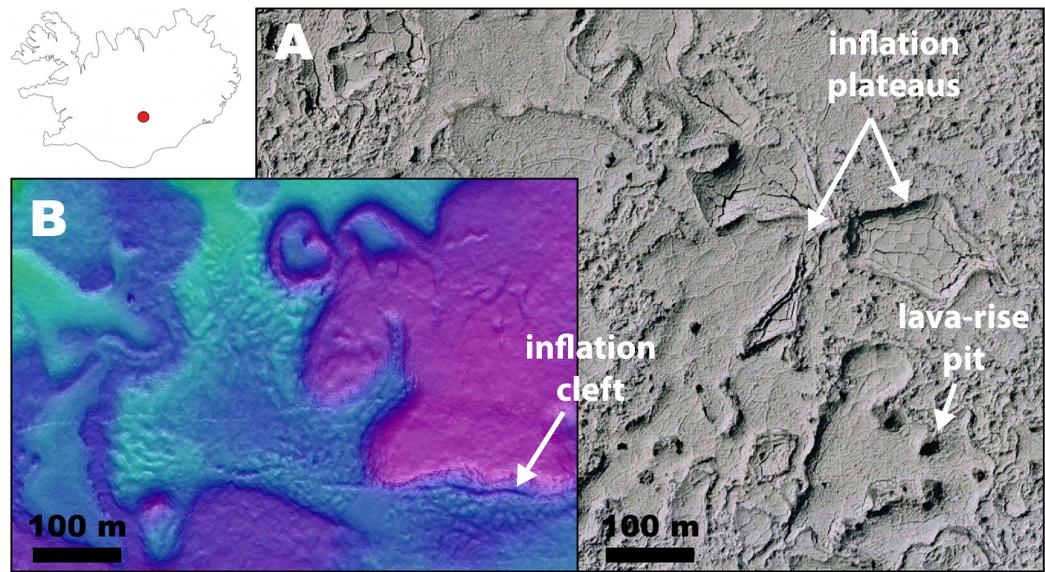
Figure 13. (a) Aerial photograph of the Brunahraun inflated lava flow field, ~300 m NNE the Eyjalon lake. The lava have been emitted from the Laki vent system, and flowed the Hverfisfljót river bed. Inflation plateaus reach ~700 m in diameter. (b) Inflated lava flows at the summit of the East Pacific Rise, 16°N, at the same scale. Data source: high-resolution (1 m cells) bathymetry acquired by the Autonomous Underwater Vehicle Aster-X (Ifremer).

inflated features emplaced in either lakes, rivers, or deep sea are similar: tumuli have lengths up to 55 m and heights up to 10 m, pressure ridges reach 2 km in length and their height exceeds 11 m. Inflation plateaus have diameters up to 1.2 km and heights up to 15 m. In contrast, lava inflation in subaerial environments form features that are typically less than few meters in height, and few hundred meters in length (most often few tens meters; Figure 15). In both subaerial and subaqueous environments, units emplaced on horizontal terrain (slope <2°, most often <1°), during a long-lived eruption, inflate due to the development of viscoelastic and brittle layers at the flow surface that counteract the internal hydraulic pressure and
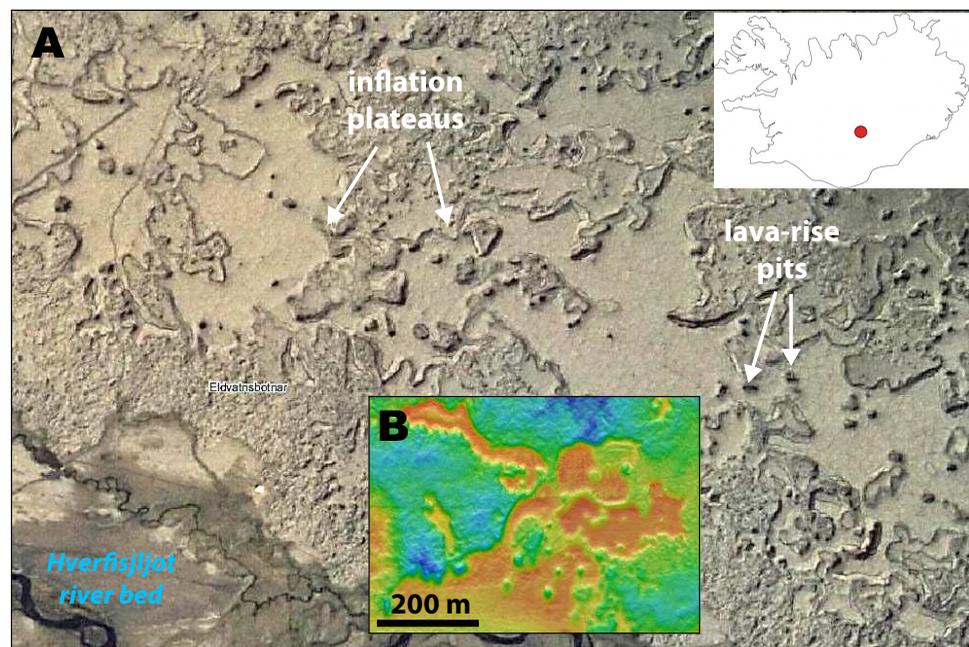
Figure 14. (a) Aerial photograph of the Brunahraun inflated lava flow field. The lava have been emitted from the Laki vent system, and flowed the Hverfisfljót river bed. Inflation plateaus reach ~800 m in diameter. (b)A 2-D view of inflated lava flows at the summit of the East Pacific Rise, 16°N, at the same scale.
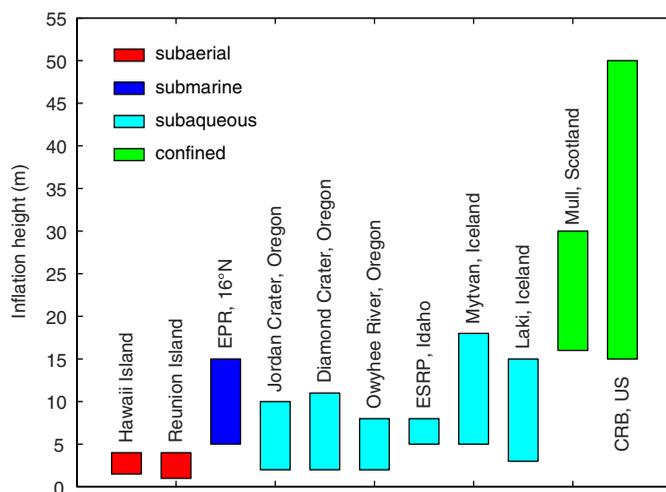
Figure 15. Range of inflation heights for plateaus in different settings. Submarine inflated flows (EPR, East Pacific Rise) are separated from the subaqueous (Western US, Iceland) such as ESRP (Eastern Snake River Province) flows. Mull and CRB (Columbia River Basalts) flows are represented as their own categories as they are potentially different (i.e., much longer lived eruptions, confined in topographic depressions).

whose tensile strength is able to retain the incoming lava. Even if this primary mechanism is similar in both types of environments, one or several key parameters influencing lava emplacement dynamics necessarily differ. In the section 6, we investigate the role of water during eruption in lava flow shaping.

6. The Role of Water in Lava Dynamics

The eruption temperature and the rate of heat loss from the surface control the formation and the thickening of this cooled layer, and together with the extrusion rate and the melt viscosity, the flow advance and

morphology [*Griffiths and Fink*, 1992b]. As lava initial temperature and composition are fairly identical for all the lava flows addressed in this study, i.e., olivine tholeiites, the most obvious difference that appears here is the emplacement of lava in a subaerial or a subaqueous environment. We compare the theoretical heat loss of a lava flow erupting in subaerial and subaqueous environments. Cooling controls the thickness of the upper brittle and viscoelastic layers, and thus likely partly controls the lava inflation process. A more efficient lava cooling in "wet" environments may result in the development of a thicker (hence stronger) upper cooled layer, which resists continued movement of the flow, whereas a thinner layer developing in aerial environment may favor lobe breakouts since internal pressure more rapidly exceeds its tensile strength. The ability of a lava flow to inflate depends on the tensile strength of the viscoelastic and brittle upper layers at the flow surface [e.g., *Hon et al.*, 1994]. Below, we compare the development of these layers in air and water with a simple model of cooling in one dimension, by computing the deepening of the 1070°C and 800°C isotherms that define the bases of the viscoelastic and brittle layers, respectively.

6.1. Heat Loss of Lava Cooling in Air and Water

In air, the heat transfer from the lava into atmosphere occurs mostly through radiative cooling, which far exceeds the heat loss by other mechanisms, especially at high temperatures [*Dragoni*, 1989; *Keszthelyi and Denlinger*, 1996; *Harris and Rowland*, 2001; *Patrick et al.*, 2004]. The radiative heat transfer can be expressed using the Stefan-Boltzmann equation:

$$Q_r = \sigma \varepsilon (T_l^4 - T_{amb}^4) \tag{1}$$

where Q_r is radiative heat flux, σ is Stefan-Boltzmann constant (5.670×10^{-8} W m^{-2} K^{-4}), and ε is emissivity of the lava surface (generally 0.90 for basalt) [e.g., *Kahle et al.*, 1988; *Crisp and Baloga*, 1990; *Salisbury and D'Aria*, 1994], T_l is the temperature of the surface of the flow, and T_{amb} is the ambient air temperature [*Kreith et al.*, 1993]. Based on this equation (1), the radiative heat loss of a basalt flow initially erupted at ~1140°C ranges from 2.3×10^3 to 1.4×10^5 W m^{-2} for a surface temperature ranging from 200 to 1000°C.

Convective heat transfer in a fluid (air or water here) occurs when temperature gradients are sufficient to generate fluid motion. Convective heat loss can be described by Newton's law of cooling:

$$Q_c = h_c (T_l - T_{amb}) \tag{2}$$

where Q_c is the convective heat flux, T_l is the temperature of the lava surface, T_{amb} is the ambient (air or water) temperature, and h_c is the heat transfer coefficient, which describes the convective vigor. A low fluid

Table 2. Parameters Used for Heat Loss Calculation Based on the Equation of Heat Diffusion

Parameter	Value
Lava flow thickness	10 m
Lava emission temperature	1140°C
Lava thermal conductivity in air (k)	1.5 W m^{-1} K^{-1}
Lava thermal conductivity in water (k)	2.5 W m^{-1} K^{-1}
Glass thermal conductivity (k)	1.25 W m^{-1} K^{-1}
Lava heat capacity	1100 J kg^{-1} K^{-1}
Lava density	2500 kg m^{-3}
Ambient temperature (in air and water)	278 K, 5°C
Emissivity in air	0.9
Emissivity in water	0
Reference temperature (T$_{ref}$)	673 K, 400°C
Reference heat transfer coefficient range in air (h$_{cref}$)	5–15 W m^{-2} K^{-1}
Reference heat transfer coefficient range in water (h$_{cref}$)	100–1000 W m^{-2} K^{-1}
Thickness of the glassy rind in air	2 mm
Thickness of the glassy rind in water	2 cm
Water energy activation (E)	14.5 kJ mol^{-1}
Gas constant (R)	8.314 J mol^{-1} K^{-1}
Sutherland's law temperature constant (T$_{air}$)	110.54 K

viscosity (η) or a high thermal gradient between the lava and the ambient fluid result in fast convective motions (high h_c) and a very efficient heat transfer. Here we relate this coefficient h_c to the thickness δ of the thermal boundary layer (TBL) at the base of the fluid: heat transfer through this thin TBL is purely conductive [e.g., *Howard*, 1964], so that:

$$h_c = k/\delta \qquad (3)$$

where k is thermal conductivity of the lava. The thickness of the boundary layer (δ) depends on the temperature change across the TBL ($\Delta T = T_l - T_{amb}$) and on the viscosity η of the ambient fluid (either air or water), which itself depends on the average temperature ($\bar{T}$) within the TBL. A boundary layer analysis [e.g., *Howard*, 1964] to express δ as a function of the temperature change and viscosity, combined with equation (3), yields:

$$h_c = h_{cref}(\Delta T/\Delta T_{ref})^{\beta}(\eta_{ref}/\eta)^{\beta} \qquad (4)$$

where the subscript *ref* is for a reference value of the temperature T_{ref} at the surface of the lava, and where the exponent β s in the range 0.25–0.33. We choose beta = 0.33 as it is the value predicted by a boundary layer analysis [e.g., *Howard*, 1964]. Hereafter, the depths of isotherms change by less than 0.5% when varying beta between 0.25 and 0.33.

The differences between convective heat transfer in air and in water are the following: (1) h_{cref} is larger in water than in air for the same temperature T_{ref} [e.g., *Patrick et al.*, 2004] and (2) the dependence of the viscosity on temperature in air and water shows a divergent trend: in air, the viscosity increases with temperature, due to higher thermal agitation, while in liquid such as water the viscosity decreases with temperature. In air, viscosity can be expressed by the Sutherland's law [*Sutherland*, 1893]:

$$\eta/\eta_{ref} = (\bar{T}/\bar{T}_{ref})^{3/2}(\bar{T}_{ref} + T_{air})/(\bar{T} + T_{air}) \qquad (5)$$

where T_{air} is the Sutherland temperature constant for air (T_{air} = 110.54 K) and $\bar{T}$ denotes the average value of the temperature within the thermal boundary layer, taken as $\bar{T} = (T_l + T_{amb})/2$.

In water, an Arrhenius law is used:

$$\eta/\eta_{ref} = exp(E/R(1/\bar{T} - 1/\bar{T}_{ref})) \qquad (6)$$

Symbol definitions and their values are given in Table 2.

The calculated values of h_c obtained using T_{ref} = 400°C, combining equations (4–6), are shown in Figure 16. In air, h_c is less dependent on the lava temperature than in the case of water, due to the increased viscosity of air at high temperatures which limits heat transfer efficiency. In water, h_c increases fairly linearly with the surface (and hence the lava) temperature.

It should be noted that we consider only free (or natural) convection that typically occurs in still conditions, when the relative velocity between the lava and the overlying fluid is close to zero (i.e., no wind in air nor current in water) [*Holman*, 1992]. Forced convection occurs when the relative velocity between the surface
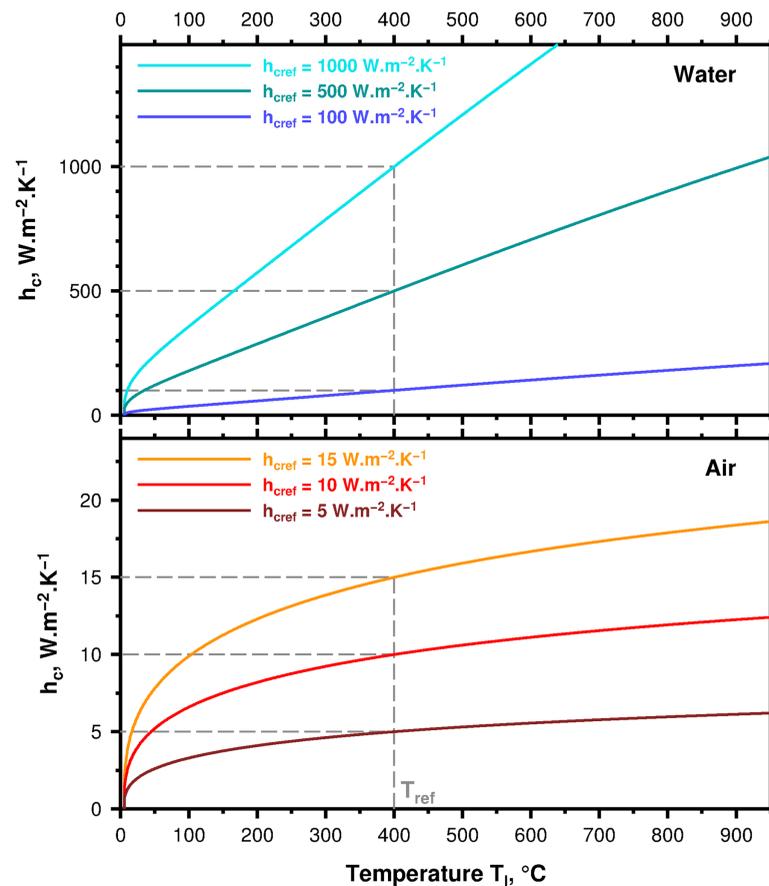
Figure 16. Heat transfer coefficient (hc), as a function of the lava surface temperature Tl, calculated using equation (4), combined with equation (5) in air (Sutherland's law for the dependence of air viscosity on temperature) and with equation (6) in water (Arrhenius-type law for the dependence of water viscosity on temperature).

of the flow and the ambient fluid is significant (i.e., wind speed above 5 m s^{-1}, for example [*Harris and Rowland*, 2001]). In air, forced convection is negligible compared to the free convective flux during the early stage of lava cooling [e.g., *Head and Wilson*, 1986; *Griffiths and Fink*, 1992b]. In water, a calculated example for the ∼4000 m deep North Arch lava flows (Hawaii), finds the forced convective heat transfer coefficient is lower by an order of magnitude compared to the free convective transfer coefficient, for surface temperature ranging 0°–600°C of basalts emplaced in 0°C waters [*Morris et al.*, 2002; *Morris*, 2003]. We thus ignore the heat loss by forced convection in this study.

We solve the heat diffusion equation in one dimension considering a 10 m thick lava layer, with a fixed temperature at the base of the layer ($T_b = 1140$°C) and an imposed heat flux at the surface given by the sum $Q_r + Q_c$, where both Q_r (equation (1)) and Q_c (equation (2)) depend on the evolving temperature T_l at the surface of the lava. Computations start with a uniform initial temperature of 1140°C across the lava layer. We consider the first 5 days (120 h) of lava cooling and under this condition, only the upper 2–3 m at most of the layer are affected by cooling, the remainder of the flow maintains a uniform temperature of 1140°C. Results are thus not affected by our chosen thickness for the lava layer.

Figure 17 shows the total heat flux in air and water for different values of h_c. It indicates that for a given surface reference temperature (e.g., 400°C), variations in h_c value do not significantly influence the total heat flux. In air, variations in h_c value influence the respective contributions of the radiative and convective flux: radiative flux largely dominates the convective flux when h_c value is below 5 W m^{-2} K^{-1}, for example, especially during the first days of cooling. In water, when above 100 W m^{-2} K^{-1}, the h_c value does not influence the total heat loss, which is instead controlled by the rate of cooling of the lava as shown by equation (2). The heat loss of the lava flow emplaced in water (∼$3.10^3 - 10^5$ W m^{-2}) exceeds

DESCHAMPS ET AL. 2144
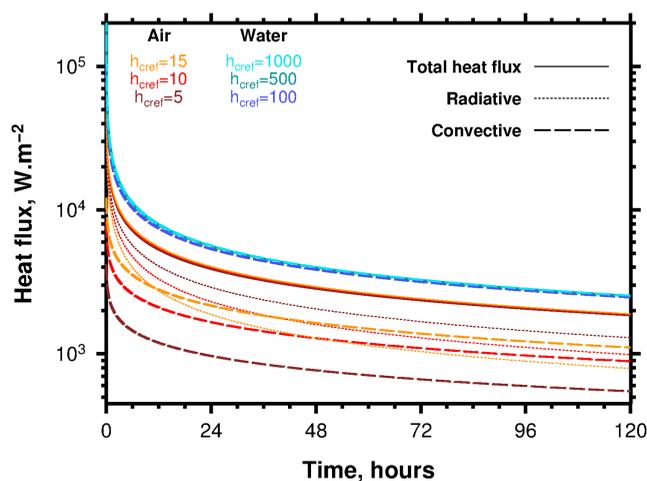
Figure 17. Heat loss in air and in water, calculated based on the heat diffusion equation in (1)-D, as a function of time, with three values of the heat transfer coefficient (h_c) in each case, assuming natural convection in both media and no radiation in water. Here lava conductivity is set at 1.5 W m^{-1} K^{-1} in air and 2.5 W m^{-1} K^{-1} in water. Convective heat flux in water is indicated for 3 h_{cref} values (100, 500, and 1000 W m^{-2} K^{-1}). The three corresponding curves are surimposed, indicating that above 100 W m^{-2} K^{-1}, the h_{cref} value does not influence significantly the cooling rate. The radiative flux is calculated based on equation (1). In air, h_{cref} value only influences the relative contributions of the radiative and convective heat loss (dotted and dashed lines, respectively), but not the value of the total heat flux (solid line).

the heat loss from a similar lava flow in air ($\sim 6.10^2 - 10^4$ W m^{-2}), implying more efficient cooling in water (Figure 17).

The method described above (equations ((1–6))) to constrain the upper thermal boundary condition of the cooling layer yields results that are consistent with previous studies. *Patrick et al.* [2004] computed values of h_c in air ranging from 3 to 10 W m^{-2} K^{-1} for lava surface temperatures ranging from 20 to 1200°C, whereas we obtain h_c between 5 and 15 W m^{-2} K^{-1} [cf. *Patrick et al.*, 2004] (Figure 4). In addition, we computed that the surface temperature of a lava emitted at a temperature of 1140°C drops to 150°C within 2 days if h_c value is 10 W m^{-2} K^{-1} in air. This agrees with the field measurements of *Hon et al.* [1994] in the

Makaopuhi inflated lava, Hawaii, whose surface temperature dropped from $\sim$1180°C to $\sim$180°C over 24 h (and remained constant for at least the next 12 days).

In water, previous studies used h_c values ranging 1300–3500 W m^{-2} K^{-1} [*Morris et al.*, 2002; *Morris*, 2003]. In the following, we calculate the deepening of the isotherms of a lava flow cooling in water using h_{cref} values ranging 100–1000 W m^{-2} K^{-1} at T_{ref} = 400°C, since heat loss does not depend on the chose value of h_{cref}, provided that it exceeds $\sim$100 W m^{-2} K^{-1} (Figure 17).

6.2. Isotherms Deepening in a Lava Flow Cooling in Air and Water

Figure 18 illustrates the importance of the lava thermal conductivity on the time-dependent depth of the cooling front. For volcanic rocks, porosity is a main controlling factor on thermal conductivity [e.g., *Horai*, 1991; *Clauser and Huenges*, 1995]. A high porosity leads to lower conductivity due to the low-conductivity fluid filling the vesicles, which can be either air or water. Hence, conductivity of Hawaiian basalts ranges from 0.1 to 2.5 W m^{-1} K^{-1}, with low-porosity basalts whose pores are filled with air and water at 1.5 and 2.5, respectively [e.g., *Horai*, 1991; *Clauser and Huenges*, 1995].

Another parameter to consider in lava cooling is the formation of a thin glassy crust at the flow surface that can insulate the lava flow due to its low thermal conductivity. This is especially so in water, due to the greater thickness of the glassy layer than in air [e.g., *Fink and Griffiths*, 1990]. Theoretical models shows that the surface of an erupting lava will reach its solidus in $\sim$10^{-3} s. Assuming a glass transition temperature of $\sim$730°C [e.g., *Ryan and Sammis*, 1981; *Griffiths and Fink*, 1992a], a 1 mm thick glassy crust will grow in only 0.2–0.7 s in water [*Griffiths and Fink*, 1992b; *Gregg and Fornari*, 1998] and in 10–12 min in air [*Hon et al.*, 1994; *Keszthelyi and Denlinger*, 1996]. Videos of subaerially erupted lava on Kilauea volcano that flowed into the ocean [*Tepley and Moore*, 1974] as well as observation of mid-ocean ridge basalts covered with a glassy rind $\sim$1–5 cm thick confirm such a chilling of the lava upper surface [e.g., *Gregg and Chadwick*, 1996]. However, Figure 19 shows that the effect of a 2 mm–5 cm thick glassy rind, whose thermal conductivity is set at 1.25 W m^{-1} K^{-1} [e.g., *Horai*, 1991] on the lava cooling is relatively limited, with only few centimeters of difference in isotherms depth after 120 h of cooling. Yet, in the following, the calculation takes into account the presence of a glassy rind 2 mm thick in air and 2 cm thick in water.

Finally, the deepening of the isotherms 800°C and 1070°C in air and water has been calculated (Figure 20) based on heat diffusion equation. Parameters used in this calculation are shown in Table 2.

Figure 18. Depth of isotherms 800°C and 1070°C calculated for a lava emplaced in air (h_{cref} value of 10 W m^{-2} K^{-1}), showing the influence of the lava thermal conductivity k (here ranging from 1.5 to 2.1 W m^{-1} K^{-1}) on the deepening of the cooling front of the 10 m thick lava flow emitted at a temperature of 1140°C.

Our calculations indicate that the isotherms that define the cooled layers deepen more quickly (by approximately 25%) when the lava emplaces into water, assuming an identical temperature of 5°C in both environments (water and air). In air, the depth of the 800 and 1070°C isotherms is approximately 38 cm and 75 cm below the lava surface after 48 h of cooling. These values are similar (within a few centimeters) to values measured directly by *Hon et al.* [1994] during subaerial Pahoehoe flow inflation at Kilauea. In water, due to more efficient cooling, the depth of the 800 and 1070°C isotherms reapproximately 55 and 105 cm below the lava surface after 48 h of cooling. To the extent that thicker crust results in greater strength, the ability of a lava flow to inflate is likely enhanced in subaqueous over subaerial environments. For similar extrusion rates, this would prevent outbreaks occurring at the margins, and result in an increased hydrostatic pressure within the lava core, promoting a greater maximum inflation of the entire flow.

6.3. Mechanical Effect of Water During Lava Emplacement

In water, the effective gravity force acting on a flow is reduced compared to the subaerial environment [*Fink and Griffiths*, 1990], due to the lower density difference between the lava and the water. The reduced gravity (g') is given by:

$$g' = g \frac{(\rho_{lava} - \rho_{water})}{(\rho_{lava} - \rho_{air})} \tag{7}$$

where *g* is the acceleration due to gravitational forces, ρ_{water} is the density of the water, and ρ_{lava} is lava density, pair is air density, which is negligible with respect to lava and water density.

For a 1000 m deep submarine environment, seawater at a temperature of 0°C has a density of 1 046 kg m^{-3}. With a lava density of 2.6 g cm^{-3}, the effective gravity is 5.93 m s^{-2}. For a shallow, subaqueous environment, fresh water at a temperature of 0°–10°C has a density of 999.8 kg m^{-3}. With the same lava density as above, the effective gravity is 6.03 m s^{-2}. The buoyancy force countering the effect of the gravity is thus significantly higher in water, whether in the deep marine environment or in the shallow waters of a lake or a river. The presence of water that fully submerges the emplaced lava will thus greatly increase the ability of a lava to inflate. A similar result was reached by *Gregg and Fornari* [1998], who calculate that a deep-sea basalt flow should be

Figure 19. Effect of a glassy crust up to 5 cm thick on the depth of the 800°C and 1070°C isotherms in a lava flow emitted at a temperature of 1140°C after 120 h of cooling, with the glass layer installed at t = 0. A heat transfer coefficient (h_{cref}) value of 500 W m^{-2} K^{-1} and thermal conductivities of 1.25 for the glass and 2.5 W m^{-1} K^{-1} for the lava have been set for these calculations.
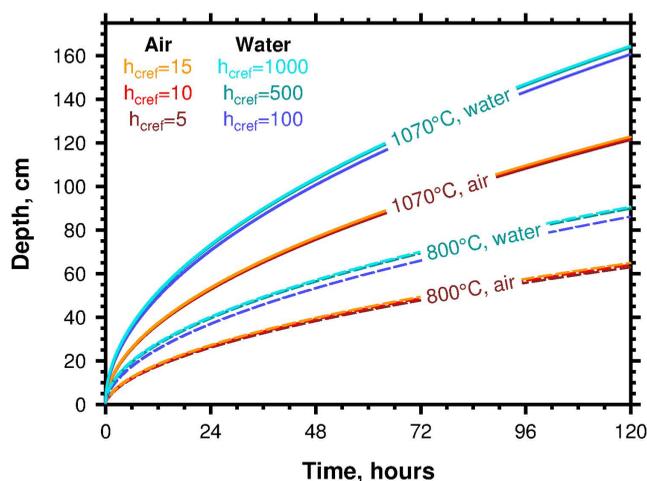
Figure 20. Depth of 800°C and 1070°C isotherms within a 10 m thick lava flow cooling in air and in water. See Table 2 for values of parameters used in the equation of heat diffusion.

roughly 30% thicker than an identical subaerial one. Hence, considering only the magma driving pressure (pushing up the lava flow) and the gravity forces per unit of the flow surface, at equilibrium (i.e., when the lava flow stops inflating), Newton's First law leads to:

$$\frac{z_{air}}{z_{water}} = \frac{(\rho_{lava} - \rho_{water})}{(\rho_{lava} - \rho_{air})} \quad (8)$$

where z is the maximum lava flow height in air and in water and ρ the density of lava, water, and air.

Equation (8) shows that for the same magma driving pressure, the buoyancy equilibrium occurs for a thicker (by 60%) lava flow when emplaced in water. In water, buoyancy thus increases the ability of a lava to swell vertically by 50%–64% depending on the lava density (2.600–3.00 g cm^{-3}, i.e., the density of liquid and solid basalts, respectively), for a similar driving pressure, regardless of the water column height and the thermodynamic effects addressed in the previous paragraph.

7. Conclusion

Our morphological study of inflated flows in different environments (air, lake, river, East Pacific Rise) reveals different geometries of inflated flows depending upon whether their deposition is in a subaqueous or in subaerial environment. Inflated structures in subaqueous environments are remarkably similar to each other in terms of geometry and size, and are characterized by tumuli with lengths up to 55 m and heights up to 10 m, pressure ridges that reach 2 km in length and 11 m in height. Inflation plateaus have diameters up to 1.2 km and heights up to 15 m. In contrast, lava inflation in aerial environments forms features that are typically less than few meters in height, and few hundred meters in length (most often few tens meters). This indicates that the water plays a major role in lava shaping, likely acting on the eruption dynamics.

Based on the equation of heat diffusion, we demonstrate that a more efficient cooling of a lava flow in water than in the air, due to vigorous convection and efficient heat transfer, leads to the development of a thicker (by approximately 25%) crust at the surface of the flow, composed of a brittle part and a visco-elastic part, the base of which being defined by the isotherms 800°C and 1070°C, respectively. Such a thicker crust in water has more strength to retain the lava than in subaerial environment, counteracting more efficiently the internal hydrostatic pressure of the flow, thus limiting breakouts of lava to form new lobes and promoting lava swelling. We show that the glassy rind that forms rapidly at the surface of the flow due to lava chilling, has only a minor influence on the depth of the cooling front (only by a few centimeters). In addition, we show that buoyancy increases the ability of a lava to swell by 60% on the condition the lava flow is fully submerged, whatever the water depth, with no thermodynamic consideration.

The presence of water can thus explain that inflated features such as tumuli, inflation plateaus, and pressure ridges are 2–3 times higher in subaqueous environments, enhanced cooling and buoyancy in water promoting lava swelling. However, we have considered in this comparative study that lava flows in air and water are similar in terms of composition, viscosity, temperature, for example, and are emplaced in the same conditions (same driving pressure) which may be valid at the first order only. Further studies are required to compute the heat exchange and progress toward thermal equilibrium when other factors are considered such as vesiculation, viscous dissipation, thermal conductivity changes, conductive cooling at the flow base, and latent heat of crystallization under varying ambient conditions existing in the eruptive

environment (e.g., changes in temperature, wind, currents, and rainfalls). Such computations have been done for lava emplaced in air [e.g., *Patrick et al.*, 2004] but not yet in water.

References

Appelgate, B., and R. W. Embley (1992), Submarine tumuli and inflated tube-fed lava flows on Axial Volcano, Juan de Fuca Ridge, *Bull. Volcanol.*, *54*(6), 447–458, doi:10.1029/JB095iB08p12765.

Bergquist, J. R., H. D. King, R. J. Blakely, D. L. Sawatzky, and J. E. Olson (1990), Mineral resources of the badlands Wilderness Study Area and the badlands Wilderness Study Area ADDITIONS, Crook and Deschutes Counties, Oregon, *U.S. Geol. Surv. Bull., 1744-B*, 14 p.

Bondre, N. R. (2006), Field and geochemical investigation of basaltic magmatism in the western United States and western India, Miami University, PhD thesis, 263 p., Miami Univ., Oxford, Ohio.

Bondre, N. R., R. A. Duraiswami, and G. Dole (2004), A brief comparison of lava flows from the Deccan volcanic province and the Columbia-Oregon plateau flood basalts: Implications for models of flood basalt emplacement, *J. Earth Syst. Sci.*, *113*(4), 809–817, doi:10.1007/BF02704039.

Brossy, C. C. (2007), Fluvial response to intra-canyon lava flows, Owyhee River, Southeastern Oregon, MS thesis, 109 p., Central Wash. Univ., Ellensburg, Wash.

Brown, G. B. (1980), Geologic and mineral resources of the Diamond Craters volcanic complex, Harney County, Oregon, with comparative data for selected areas of volcanism in Oregon and Idaho, *Mineral Rep. Serial OR 10676*, 30 p., U.S. Bureau of Land Management, Oreg.

Calzia, J. P., S. Hubbard-Sharpless, R. L. Turner, A. Griscom, and D. L. Sawatzky (1988), Mineral resources of the Jordan Craters Wilderness Study Area, Malheur County, Oregon, *U.S. Geol. Surv. Open File Rep.*, *88*(572), 11 p.

Carbotte, S. M., A. Solomon, and G. Ponce-Correa (2000), Evaluation of morphological indicators of magma supply and segmentation from a seismic reflection study of the East Pacific Rise 15°30′–17°N, *J. Geophys. Res.*, *105*(B2), 2737–2759, doi:10.1029/1999JB900245.

Cashman, K. V., and J. P. Kauahikaua (1997), Reevaluation of vesicle distributions in basaltic lava flows, *Geology*, *25*(5), 419–422, doi:10.1130/0091-7613.

Cashman, K. V., C. Thornber, and J. P. Kauahikaua (1999), Cooling and crystallization of lava in open channels, and the transition of Pāhoehoe Lava to'A'ā, *Bull. Volcanol.*, *61*(5), 306–323, doi:10.1007/s004450050299.

Chadwick, W. W., R. W. Embley, H. B. Milburn, C. Meinig, and M. Stapp (1999), Evidence for deformation associated with the 1998 eruption of Axial Volcano, Juan de Fuca Ridge, from acoustic extensometer measurements, *Geophys. Res. Lett.*, *26*(23), 3441–3444, doi:10.1029/1999GL900498.

Chadwick, W. W., D. A. Clague, R. W. Embley, M. R. Perfit, D. A. Butterfield, D. W. Caress, J. B. Paduan, J. F. Martin, P. Sasnett, and S. G. Merle (2013), The 1998 eruption of Axial Seamount: New insights on submarine lava flow emplacement from high-resolution mapping, *Geochem. Geophys. Geosyst.*, *14*, 3939–3968, doi:10.1002/ggge.20202.

Chitwood, L. A. (1990), Devils Garden, Oregon, in *Volcanoes of North America: United States and Canada*, edited by C. A. Wood and J. Kienle, p. 203, Cambridge Univ. Press, N. Y.

Chitwood, L. A. (1994), Inflated basaltic lava—Examples of processes and landforms from central and southeast Oregon, *Oreg. Geol.*, *56*(1), 11–21.

Clauser, C., and E. Huenges (1995), Thermal conductivity of rocks and minerals, in *Rock Physics and Phase Relations: A Handbook of Physical Constants*, vol. 3, pp. 105–126, AGU, San Francisco, Calif.

Cormier, M.-H., K. C. Macdonald, and D. S. Wilson (1995), A three-dimensional gravity analysis of the East Pacific Rise from 18 degrees to 21 degrees 30′S, *J. Geophys. Res.*, *100*(B5), 8063–8082, doi:10.1029/95JB00243.

Crisp, J., and S. Baloga (1990), A model for lava flows with two thermal components, *J. Geophys. Res.*, *95*(B2), 1255–1270, doi:10.1029/JB095iB02p01255.

Deschamps, A., M. A. Tivey, W. W. Chadwick Jr., and R. W. Embley (2013), Waning magmatic activity along the Southern Explorer Ridge revealed through fault restoration of rift topography, *Geochem. Geophys. Geosyst.*, *14*, 1609–1625, doi:10.1002/ggge.20110.

Dragoni, M. (1989), A dynamical model of lava flows cooling by radiation, *Bull. Volcanol.*, *51*(2), 88–95, doi:10.1007/BF01081978.

Dugas, D. P. (1998), Late quaternary variations in the level of paleo-lake Malheur, eastern Oregon, *Quat. Res.*, *50*(3), 276–282, doi:10.1006/qres.1998.2005.

Duraiswami, R. A., N. R. Bondre, G. Dole, V. M. Phadnis, and V. S. Kale (2001), Tumuli and associated features from the western Deccan Volcanic Province, India, *Bull. Volcanol.*, *63*(7), 435–442, doi:10.1007/s004450100160.

Einarsson, A. (1982), The palaeolimnology of Lake Mỳvatn, northern Iceland: Plant and animal microfossils in the sediment, *Freshwater Biol.*, *12*(1), 63–82.

Einarsson, Á. (1991), Lífríki í 2000 ár, in *Náttúra Myvatns Hid íslenska Náttúrufrædifélag, Reykjavík*, edited by A. Gardarsson and Á. Einarsson, in Náttúra Mývatns, pp. 320–336.

Einarsson, Á., G. Stefánsdóttir, H. Jóhannesson, J. S. Ólafsson, G. M. Gíslason, I. Wakana, G. Gudbergsson, and A. Gardarsson (2004), The ecology of Lake Myvatn and the River Laxá: Variation in space and time, *Aquat. Ecol.*, *38*(2), 317–348.

Ely, L. L., C. C. Brossy, P. K. House, E. B. Safran, J. E. O'Connor, D. E. Champion, C. R. Fenton, N. R. Bondre, C. A. Orem, and G. E. Grant (2012), Owyhee River intracanyon lava flows: Does the river give a dam?, *Geol. Soc. Am. Bull.*, *124*(11–12), 1667–1687, doi:10.1130/B30574.1.

Evans, J. G. (1991), Geologic map of the lower Owyhee Canyon Wilderness Study Area, Malheur County, Oregon, in *U.S. Geological Survey Miscellaneous Field Studies, Map MF-2167*, sheet 1, scale 1:48,000

Fink, J. H., and R. W. Griffiths (1990), Radial spreading of viscous-gravity currents with solidifying crust, *J. Fluid Mech.*, *221*(1), 485–509, doi:10.1017/S0022112090003640.

Fornari, D. J. (1986), Submarine lava tubes and channels, *Bull. Volcanol.*, *48*(5), 291–298, doi:10.1007/BF01081757.

Garel, F., E. Kaminski, S. Tait, and A. Limare (2012), An experimental study of the surface thermal signature of hot subaerial isoviscous gravity currents: Implications for thermal monitoring of lava flows and domes, *J. Geophys. Res.*, *117*, B02205, doi:10.1029/2011JB008698.

Greeley, R. (1982), The style of basaltic volcanism in the eastern Snake River Plain, Idaho, *Cenozoic Geol. Idaho*, *26*, 407.

Greeley, R., and S. A. Fagents (2001), Icelandic pseudocraters as analogs to some volcanic cones on Mars, *J. Geophys. Res.*, *106*(E9), 20,527–20,546, doi:10.1029/2000JE001378.

Gregg, T. K., and W. W. Chadwick (1996), Submarine lava-flow inflation: A model for the formation of lava pillars, Geology, 24(11), 981–984, doi:10.1130/0091-7613(1996).

Gregg, T. K., and D. J. Fornari (1998), Long submarine lava flows: Observations and results from numerical modeling, *J. Geophys. Res.*, *103*(B11), 27,517–27,531, doi:10.1029/98JB02465.

Griffiths, R. W., and J. H. Fink (1992a), The morphology of lava flows in planetary environments: Predictions from analog experiments, *J. Geophys. Res.*, *97*(B13), 19,739–19,748, doi:10.1029/92JB01953.

Griffiths, R. W., and J. H. Fink (1992b), Solidification and morphology of submarine lavas: A dependence on extrusion rate, *J. Geophys. Res.*, *97*(B13), 19,729–19,737, doi:10.1029/92JB01594.

Grönvold, K (1984), The petrochemistry of the Laki lava flow, edited by G.A. Gunnlaugsson and S Rafnsson Skaftáreldar, 1783–1784: Ritgerdir og heimildir, Mal og Menning, Reykjavík: 49–58. (In Icelandic)

Guilbaud, M.-N., S. Blake, T. Thordarson, and S. Self (2007), Role of syn-eruptive cooling and degassing on textures of lavas from the AD 1783–1784 Laki eruption, South Iceland, *J. Petrol.*, *48*(7), 1265–1294, doi:10.1093/petrology/egm017.

Harris, A. J., and S. Rowland (2001), FLOWGO: A kinematic thermo-rheological model for lava flowing in a channel, *Bull. Volcanol.*, *63*(1), 20–44, doi:10.1007/s004450000120.

Hart, W. K., and S. A. Mertzman (1983), Late Cenozoic volcanic stratigraphy of the Jordan Valley area, *southeastern Oregon: Oregon Geology*, *45*(2), 15–19.

Hart, W. K., J. L. Aronson, and S. A. Mertzman (1984), Areal distribution and age of low-K, high-alumina olivine tholeiite magmatism in the northwestern Great Basin, *Geol. Soc. Am. Bull.*, *95*(2), 186–195, doi:10.1130/0016–7606.

Head, J. W., and L. Wilson (1986), Volcanic processes and landforms on Venus: Theory, predictions, and observations, *J. Geophys. Res.*, *91*(B9), 9407–9446, doi:10.1029/JB091iB09p09407.

Helo, C., D. A. Clague, D. B. Dingwell, and J. Stix (2013), High and highly variable cooling rates during pyroclastic eruptions on Axial Seamount, Juan de Fuca Ridge, *J. Volcanol. Geotherm. Res.*, *253*, 54–64, doi:10.1016/j.jvolgeores.2012.12.004.

Hoblitt, R. P., T. R. Orr, C. Heliker, R. P. Denlinger, K. Hon, and P. F. Cervelli (2012), Inflation rates, rifts, and bands in a pāhoehoe sheet flow, *Geosphere*, *8*(1), 179–195.

Holcomb, R. T. (1981), Kilauea Volcano, Hawaii: Chronology and morphology of the surficial lava flows, *U.S. Geol. Surv. Open File Rep.*, *81*(354), 321.

Holman, J. P. (1992), *Heat Transfer*, (Mech. Eng. McGraw-Hill Ser.), 713 pp., McGraw-Hill Education, New York.

Hon, K., and J. Kauahikaua (1991), The importance of inflation in the formation of pahoehoe sheet flows, *Eos Trans. AGU*, *72*, 557.

Hon, K., J. Kauahikaua, R. Denlinger, and K. Mackay (1994), Emplacement and inflation of pahoehoe sheet flows: Observations and measurements of active lava flows on Kilauea Volcano, Hawaii, *Geol. Soc. Am. Bull.*, *106*(3), 351–370.

Hooper, P. R. (1982), The Columbia river basalts, *Science*, *215*(4539), 1463–1468, doi:10.1126/science.215.4539.1463.

Hooper, P. R. (2000), Chemical discrimination of Columbia River basalt flows, *Geochem. Geophys. Geosyst.*, *1*(6), 1024, doi:10.1029/2000GC000040.

Horai, K. (1991), Thermal conductivity of Hawaiian basalt: A new interpretation of Robertson and Peck's data, *J. Geophys. Res.*, *96*(B3), 4125–4132, doi:10.1029/90JB02452.

Howard, L. N. (1964), Convection at high Rayleigh number, in *Applied Mechanics, Proceedings of 11th Congress of Applied Mathematics*, edited by H. Görtler, pp. 1109–1115, Springer, Berlin, doi:10.1007/978-3-662–29364-5_147.

Hughes, S. S., R. P. Smith, W. R. Hackett, and S. R. Anderson (1999), Mafic volcanism and environmental geology of the eastern Snake River Plain, Idaho, in *Guidebook to the Geology of Eastern Idaho*, edited by S. S. Hughes and G. D. Thackray, pp. 143–168, Idaho Mus. of Nat. Hist., Pocatello, Idaho Museum of Natural History.

James, M., N. Bagdassarov, K. Müller, and H. Pinkerton (2004), Viscoelastic behaviour of basaltic lavas, *J. Volcanol. Geotherm. Res.*, *132*(2–3), 99–113, doi:10.1016/S0377-0273(03)00340-8.

Jensen, R. A. (2006), *Roadside Guide to the Geology of Newberry Volcano*, 4th edition: Bend, Oregon, CenOreGeoPub, 182 p.

Jones, J. G. (1968), Pillow lava and pahoehoe, *J. Geol.*, *76*(4), 485–488.

Jones, J. G., and P. H. H. Nelson (1970), The flow of basalt lava from air into water—its structural expression and stratigraphic significance: *Geological Magazine*, *107*(1), 13–19.

Kahle, A. B., A. R. Gillespie, E. A. Abbott, M. J. Abrams, R. E. Walker, G. Hoover, and J. P. Lockwood (1988), Relative dating of Hawaiian lava flows using multispectral thermal infrared images: A new tool for geologic mapping of young volcanic terranes, *J. Geophys. Res.*, *93*(B12), 15,239–15,251, doi:10.1029/JB093iB12p15239.

Kauahikaua, J., K. V. Cashman, T. N. Mattox, C. C. Heliker, K. A. Hon, M. T. Mangan, and C. R. Thornber (1998), Observations on basaltic lava streams in tubes from Kilauea Volcano, island of Hawaii, *J. Geophys. Res.*, *103*(B11), 27,303–27,323, doi:10.1029/97JB03576.

Keith, W. J., H. D. King, M. E. Gettings, and F. L. Johnson (1988), Mineral resources of the Devil's Garden Lava Bed, Squaw Ridge Lava Bed, and four Craters Lava Bed Wilderness Study Areas, Lake County, Oregon, *U.S. Geol. Surv. Bull.*, *1738-A*, 14.

Kent, R. W., B. A. Thomson, R. R. Skelhorn, A. C. Kerr, M. J. Norry, and J. N. Walsh (1998), Emplacement of Hebridean tertiary flood basalts: Evidence from an inflated pahoehoe lava flow on Mull, Scotland, *J. Geol. Soc. London*, *155*(4), 599–607.

Keszthelyi, L., and R. Denlinger (1996), The initial cooling of pahoehoe flow lobes, *Bull. Volcanol.*, *58*(1), 5–18, doi:10.1007/s004450050121.

Keszthelyi, L., T. Thordarson, A. McEwen, H. Haack, M.-N. Guilbaud, S. Self, and M. J. Rossi (2004), Icelandic analogs to Martian flood lavas, *Geochem. Geophys. Geosyst.*, *5*, Q11014, doi:10.1029/2004GC000758.

Kreith, F., M. S. Bohn, and R. D. Ulrich (1993), *Principles of Heat Transfer*, 5th ed., 646 p., West Publ. Co., Minneapolis/St. Paul.

Kuntz, M. A., D. E. Champion, E. C. Spiker, R. H. Lefebvre, and L. A. McBroome (1982), The Great Rift and the evolution of the Craters of the Moon lava field, Idaho, *Idaho Bureau of Mines and Geology Bulletin*, *26*, 423–437.

Kuntz, M. A., H. R. Covington, and L. J. Schorr (1992), An overview of basaltic volcanism of the eastern Snake River Plain, Idaho, in *Regional Geology of Eastern Idaho and Western Wyoming, Geol. Soc. Am. Mem. 179*, edited by P. K. Link, M. A. Kuntz, and L. B. Platt, pp. 227–267.

Leeman, W. P. (1982), Evolved and hybrid lavas from the Snake River Plain, Idaho, in Cenozoic Geology of Idaho, edited by B. Bonnichsen and R. M. Breckenridge, *Idaho Bureau of Mines and Geology Bulletin*, *26*, 193–202.

Lenat, J.-F., P. Bachelery, and F. Desmulier (2001), Genese du champ de lave de l'Enclos Fouque; une eruption d'envergure exceptionnelle du Piton de la Fournaise (Reunion) au 18 e siecle, *Bull. Soc. Géol. Fr.*, *172*(2), 177–188.

Lyle, P. (2000), The eruption environment of multi-tiered columnar basalt lava flows, *J. Geol. Soc. London*, *157*(4), 715–722.

Macdonald, G. A. (1953), Pahoehoe, aa, and block lava, *Am. J. Sci.*, *251*(3), 169–191.

Mattsson, H. B., and Á. Höskuldsson (2011), Contemporaneous phreatomagmatic and effusive activity along the Hverfjall eruptive fissure, north Iceland: Eruption chronology and resulting deposits, *J. Volcanol. Geotherm. Res.*, *201*(1), 241–252.

McClinton, T., S. M. White, A. Colman, and J. M. Sinton (2013), Reconstructing lava flow emplacement processes at the hotspot-affected Galápagos spreading center, 95° W and 92° W, *Geochem. Geophys. Geosyst.*, *14*, 2731–2756, doi:10.1002/ggge.20157.

Morris, A. R. (2003), Emplacement of deep submarine lava flows on the North Hawaiian Arch: A study of thermal and rheological evolution using a numerical model, MS thesis, 125 pp., Numéro 3779, de Theses for the degree of Master of Science (University of Hawaii at Manoa): Geology and Geophysics, Univ. of Hawaii.

Morris, A. R., A. J. Harris, B. Appelgate, and S. K. Rowland (2002), Understanding the thermal and rheological evolution of deep submarine lava flows in the North Arch Volcanic Field, *Eos Trans. AGU*, *1*(04), Fall Meet. Suppl., Abstract V62D-04.

Ólafsson, J. (1979), Physical characteristics of Lake Mỳvatn and River Laxá, *Oikos*, *32*, 38–66.

Orem, C. A. (2010), Lacustrine sediment record of multiple quaternary lava dams on the Owyhee River, Southeastern Oregon, MS thesis, 137 p., Central Wash. Univ., Ellensburg, Wash.

Orem, C. A., L. L. Ely, C. C. Brossy, P. K. House, J. E. O'Connor, and E. Safran (2011), Sedimentological analysis of the West Crater lake: Insights into processes of lava dam formation, lake sedimentation, and river incision, *Geological Society of America Abstracts with Programs*, *43*(4), 52.

Otto, B. R., and D. A. Hutchison (1977), The geology of Jordan Craters, Malheur County, Oregon, *Ore Bin*, *39*(8), 125–140.

Patrick, M. R., J. Dehn, and K. Dean (2004), Numerical modeling of lava flow cooling applied to the 1997 Okmok eruption: Approach and analysis, *J. Geophys. Res.*, *109*, B03202, doi:10.1029/2003JB002537.

Pearson, D. G., C. H. Emeleus, and S. P. Kelley (1996), Precise 40Ar/39Ar age for the initiation of Palaeogene volcanism in the Inner Hebrides and its regional significance, *J. Geol. Soc. London*, *153*(6), 815–818.

Peterson, N. V., and E. A. Groh (1964), Diamond Craters, Oregon, *Ore Bin*, *26*(2), 17–34.

Rossi, M. J., and A. Gudmundsson (1996), The morphology and formation of flow-lobe tumuli on Icelandic shield volcanoes, *J. Volcanol. Geotherm. Res.*, *72*(3), 291–308.

Rowland, S. K., A. J. Harris, M. J. Wooster, F. Amelung, H. Garbeil, L. Wilson, and P. J. Mouginis-Mark (2003), Volumetric characteristics of lava flows from interferometric radar and multispectral satellite data: The 1995 Fernandina and 1998 Cerro Azul eruptions in the western Galapagos, *Bull. Volcanol.*, *65*(5), 311–330.

Russell, J. K., and J. Nicholls (1987), Early crystallization history of alkali olivine basalts, Diamond Craters, Oregon, *Geochim. Cosmochim. Acta*, *51*(1), 143–154.

Ryan, M. P., and C. G. Sammis (1981), The glass transition in basalt, *J. Geophys. Res.*, *86*(B10), 9519–9535.

Sæmundsson, K. (1991), Jardfrædi Kröflukerfisins, in *Náttúra Myvatns*, edited by A. Gardarsson and Á. Einarsson, pp. 24–95, Hid íslenska Náttúrufrædifélag, Reykjavík, Iceland.

Sakimoto, S. E. H., and M. T. Zuber (1998), Flow and convective cooling in lava tubes, *J. Geophys. Res.*, *103*(B11), 27,465–27,487.

Salisbury, J. W., and D. M. D'Aria (1994), Emissivity of terrestrial materials in the 3–5 μm atmospheric window, *Remote Sens. Environ.*, *47*(3), 345–361.

Scheirer, D. S., and K. C. Macdonald (1993), Variation in cross-sectional area of the axial ridge along the East Pacific Rise; evidence for the magmatic budget of a fast spreading center, *J. Geophys. Res.*, *98*(B5), 7871–7885, doi:10.1029/93JB00015.

Schmincke, H.-U. (1967), Stratigraphy and petrography of four upper Yakima Basalt flows in south-central Washington, *Geol. Soc. Am. Bull.*, *78*(11), 1385–1422, doi:10.1130/0016–7606.

Self, S., S. Finnemore, Th. Thordarson, and G. P. L. Walker (1991), Importance of compound lava and lava-rise mechanisms in emplacement of flood basalts, *Eos Trans. AGU*, *72*(44), Fall Meet. Suppl., 566.

Self, S., T. Thordarson, L. Keszthelyi, G. P. L. Walker, K. Hon, M. T. Murphy, P. Long, and S. Finnemore (1996), A new model for the emplacement of Columbia River basalts as large, inflated pahoehoe lava flow fields, *Geophys. Res. Lett.*, *23*(19), 2689–2692.

Self, S., T. Thordarson, and L. Keszthelyi (1997), Emplacement of continental flood basalt lava flows, In: *Large Igneous Provinces: Continental, Oceanic, and Planetary Flood Volcanism, Geophys. Monogr. Ser.*, edited by J.J. Mahoney, and M. Coffin, pp. 381–410, AGU, Washington, D. C.

Self, S., L. Keszthelyi, and T. Thordarson (1998), The importance of pahoehoe, *Annu. Rev. Earth Planet. Sci.*, *26*(1), 81–110.

Sherrod, D. R., D. E. Champion, and J. P. McGeehin (2012), Age and duration of volcanic activity at Diamond Craters, southeastern Oregon, *J. Volcanol. Geotherm. Res.*, *247–248*, 108–114, doi:10.1016/j.jvolgeores.2012.08.008.

Sigmarsson, O., M. Condomines, K. Grönvold, and T. Thordarson (1991), Extreme magma homogeneity in the 1783–84 Lakagigar eruption: Origin of a large volume of evolved basalt in Iceland, *Geophys. Res. Lett.*, *18*(12), 2229–2232.

Steingrímsson, J. (1998), *Fires of the Earth: The Laki Eruption 1783–1784*, edited by Haskolautgafan, translated by K. Kunz, 93 pp., Univ. of Iceland Press, Reykjavik, Iceland.

Sutherland, W. (1893), The viscosity of gases and molecular force, *Philos. Mag.*, *36*(223), 507–531.

Swanson, D. A., T. L. Wright, and R. T. Helz (1975), Linear vent systems and estimated rates of magma production and eruption for the Yakima Basalt on the Columbia Plateau, *Am. J. Sci.*, *275*(8), 877–905.

Tepley, L., and J. G. Moore (1974), *Fire under the Sea: The Origin of Pillow Lava*, Moonlight Prod., Mountain View, Calif.

Thorarinsson, S. (1979), The postglacial history of the Mỳvatn area, *Oikos*, *32*, 17–28.

Thordarson, T., and A. Hoskuldsson (2002), *Iceland (Classic Geology in Europe)*, 208 pp., Dunedin Acad. Press, Edinburgh, U. K.

Thordarson, T., and S. Self (1993), The Laki (Skaftár Fires) and Grímsvötn eruptions in 1783–1785, *Bull. Volcanol.*, *55*(4), 233–263.

Thordarson, T., and S. Self (1996), Sulfur, chlorine and fluorine degassing and atmospheric loading by the Roza eruption, Columbia River Basalt Group, Washington, USA, *J. Volcanol. Geotherm. Res.*, *74*(1), 49–73.

Thordarson, T., and S. Self (1998), The Roza Member, Columbia River Basalt Group: A gigantic pahoehoe lava flow field formed by endogenous processes?, *J. Geophys. Res.* *103*(B11), 27,411–27,445, doi:10.1029/98JB01355.

Thordarson, T., S. Self, N. Oskarsson, and T. Hulsebosch (1996), Sulfur, chlorine, and fluorine degassing and atmospheric loading by the 1783–1784 AD Laki (Skaftár Fires) eruption in Iceland, *Bull. Volcanol.*, *58*(2–3), 205–225.

Tolan, T., S. Reidel, M. Beeson, J. Anderson, K. Fecht, and D. Swanson (1989), Revisions to the estimates of areal extent and volume of the Grande Ronde Basalt Group, *Geol. Soc. Am. Spec. Pap.*, *239*, 1–20.

Turcotte, D. L., and G. Schubert (1982), *Geodynamics*, vol. 450, 50 pp., John Wiley, New York.

Walker, G. P. (1991), Structure, and origin by injection of lava under surface crust, of tumuli,"lava rises","lava-rise pits", and "lava-inflation clefts" in Hawaii, *Bull. Volcanol.*, *53*(7), 546–558.

Walker, G. P. (1992), Morphometric study of pillow-size spectrum among pillow lavas, *Bull. Volcanol.*, *54*(6), 459–474, doi:10.1007/BF00301392.

Walker, G. P. L. (1971), Compound and simple lava flows and flood basalts, *Bull. Volcanol.*, *35*(3), 579–590, doi:10.1007/BF02596829.

Wang, X., J. R. Cochran, and G. A. Barth (1996), Gravity anomalies, crustal thickness, and the pattern of mantle flow at the fast spreading East Pacific Rise, 9 degrees −10 degrees N; evidence for three-dimensional upwelling, *J. Geophys. Res.*, *101*(B8), 17, doi:10.1029/96JB00194.

Wantim, M. N., M. Kervyn, G. G. J. Ernst, M. A. del Marmol, C. E. Suh, and P. Jacobs (2013), Numerical experiments on the dynamics of channelised lava flows at Mount Cameroon volcano with the FLOWGO thermo-rheological model, *J. Volcanol. Geotherm. Res.*, *253*, 35–53, doi:10.1016/j.jvolgeores.2012.12.003.

Wood, C. A., and J. Kienle (1992), *Volcanoes of North America: The United States and Canada*, 354 pp., Cambridge Univ. Press, U. K.

Wright, T. L., and R. T. Okamura (1977), *Cooling and Crystallization of Tholeiitic Basalt, 1965 Makaopuhi Lava Lake, Hawaii*, 78 pp., U.S. Gov. Print. Off., Washington.